# Mobility analysis of tripod scissor structures using screw theory

Yuan Liao [a], Gökhan Kiper [b], Sudarshan Krishnan [a, *]

[a] School of Architecture, University of Illinois at Urbana-Champaign, Champaign, USA
[b] Department of Mechanical Engineering, İzmir Institute of Technology, İzmir, Turkey
*Corresponding author. E-mail: skrishnn@illinois.edu

## Abstract

Mechanisms consisting of spatial scissor units have different kinematic behaviors than those of planar scissors. However, their kinematics, especially the mobility analysis, has not received enough attention. Two types of deployable assemblies are analyzed in this paper, namely the translational and mirrored assemblies. Both the assemblies are made of tripod scissor units, and their instantaneous mobility are examined using screw theory. The study starts on the configuration where all the members have the identical deployment angle. Firstly, the geometric property of each assembly was studied. Then, screw-loop equations were developed based on graph theory and closure equations. Finally, the mobility of each assembly was computed using linear algebra. Following the analysis, physical prototypes were constructed to validate the results, and several different motion modes were obtained for the translational assembly. The analysis reveals different kinematic behaviors of the two assemblies. In the given configuration, the translational assemblies have four instantaneous degrees of freedom, while the mirrored assemblies have only a single instantaneous degree of freedom.

**Keywords**: Deployable structures, tripod scissor, mobility, screw theory, translational assembly, mirrored assembly, kinematics.

## Nomenclature

| Symbol | Description |
|---|---|
| $k$ | Length of the lower segment of the member in a tripod scissor unit (TSU) |
| $l$ | Length of the upper segment of the member in a TSU |
| $l'$ | Theoretical length of the upper segment of the members in a mirrored TSU assembly |
| $M$ | Mobility of an assembly |
| $r_1$ | The radius of a central hub, i.e. the offset distance of the member from the central axis |
| $r_2$ | Length of the extension plates of a top or bottom hub |
| $\mathbf{R}$ | A rotation matrix |
| $\mathbf{S}$ | A screw (Jacobian) matrix |
| $\mathbf{T}$ | A translation matrix |
| $\boldsymbol{p_i}$ | Arm vector of the $i^{th}$ screw |
| $\boldsymbol{q_i}$ | Unit orientation vector of the $i^{th}$ screw |
| $\gamma$ | Deployment angle of a member from the folded state |
| $\omega_i$ | Angular speed of the $i^{th}$ revolute joint |
| $\boldsymbol{\Omega}$ | Angular velocity column matrix |
| $\boldsymbol{\$_i}$ | Screw of the $i^{th}$ revolute joint |

## 1. Introduction

Deployable structures based on scissor-like elements (SLEs) have attracted great attention from engineers and architects since the nineteenth century. Recently, scissor deployable structures have been applied to the fields of mechanical engineering [1–5] and building design [6–9] due to their special characteristics of scalability and transformability. Therefore, kinematic study is an indispensable part of the design and application of these structures.

Various types of scissor units have been developed [10]. In general, they can be classified into two categories: planar units and spatial units. Planar units typically have two members connected by a hinge and rotate about a specific axis, as shown in Fig 1a. Spatial units, on the other hand, consist of multiple members (≥ 3) that unfold in three-dimensional space, as shown in Fig. 1b. In addition, an intermediate hub is necessary to connect the scissor members at the center of the unit. Spatial units employ more members and non-parallel joint axes, making their kinematic analysis more complex than planar units.

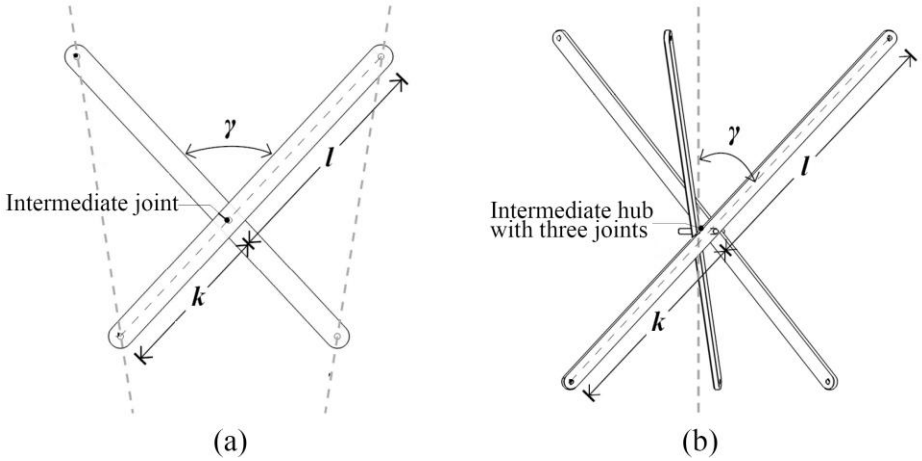


Figure 1. (a) A planar scissor unit, and (b) a spatial scissor unit with three members.

Kinematic studies of scissor mechanisms followed various geometric designs. Langbecker [11] presented a kinematic analysis of scissor structures developed by Escrig et al. [12] and Hoberman [13], and formulated the geometric condition of foldability. Patel and Ananthasuresh explained the kinematic concept of Hoberman's deployable ring, and proved the feasibility of using multi-segment members to replace several single-segment elements [14]. Chen et al. analyzed four types of planar scissor linkages with the consideration of the inherent symmetry and proposed the integral mechanism modes[15].

Dai et al. pioneered the mobility study of scissor structures [16]. He stated the difficulty of using Grübler–Kutzbach criterion to analyze the mobility of the scissor mechanisms and used screw theory for the analysis. Mao et al. reported the mobility conditions of single-loop deployable linkages [17]. Zhao et al. analyzed the mobility of spatial grids made of straight planar units, including flat, cylindrical, and spherical forms [18]. Cai et al. presented the kinematic and mobility analysis of angulated scissor rings using screw theory [19,20]. Sun et al. investigated multi-loop deployable modules consisting of planar scissor units based on screw theory and closure equation [21,22]. This method was also employed by Han et al. to examine the kinematics of scissor ring trusses designed for space antennas [23,24]. Wang et al. analyzed the mobility, motion path, and limit point of a series of planar linkages using the system constraint equations [25]. Liu et al.

employed screw theory to investigate the kinematics of a reconfigurable mechanism using SLEs [26,27]. Meng et al. studied kinematics a series of deployable ring trusses based on SLEs using screw theory [28,29].

The aforementioned literature has studied the kinematics of structures made of planar scissor units. However, the research on spatial units has focused only on their geometric design, while their kinematic study has not been thoroughly investigated yet. The design and application of spatial scissor units in architecture were pioneered by Piñero [30] who created several models of movable theaters. Escrig compared the spatial scissor units with planar ones and summarized their geometric characteristics [31]. Akgün et al. introduced four-legged spatial scissors by using additional hinges to gain more degrees of freedom (DOFs) and diverse curvilinear forms [32]. Recently, Ramos-Jaime and Sánchez-Sánchez developed design equations for spatial units and demonstrated their self-locking behavior using the concept of reciprocal structures [33]. Pérez-Valcárcel et al. applied the reciprocal-frame-like connection to the end joints, which gives a better structural performance [34,35]. Liao and Krishnan proposed a mirror assembly approach for tripod scissor units, which can achieve different forms and transformations [36,37]. Pérez-Egea et al. compared the deployable modules using both the spatial and planar units and examined the influence of joint eccentricity [38]. Suthar and Jung designed a foldable robot arm based on spatial scissor units to achieve better bending deformation compared to the traditional planar scissor structures [1,39].

The queries about the kinematic behavior of mechanisms using spatial units have been raised decades ago. Ron Resch showed in his *Paper and Stick Film* that the tripod scissor assemblies can be folded from different directions, which reveals the multiple DOFs of such mechanisms. Langbecker also pointed out that the kinematic property he developed may not apply to spatial scissor units [11]. However, the mobility of spatial scissor units has not been systematically analyzed yet. This has hindered the structure from a broader range of applications. Therefore, the gap should be filled by studying the kinematic property of spatial units.

This study presents mobility analyses of deployable assemblies composed of three-bar scissor bundle modules. These bundle modules can be deployed into a tripod [30], as shown in Fig. 1b. Therefore, they are referred to in this paper as tripod scissor units (hereafter referred to as TSUs). Screw theory is employed in this study because it has been effectively applied to examine the mobility of planar scissor units [16–22] and other complex mechanisms [40–47]. Sections 2 and Section 3 analyze the mobility of translational and mirrored assemblies, respectively. In Section 4, the results of Sections 2 and 3 are validated using physical models. Section 5 concludes the results and observations.

## 2. Mobility analysis of translational assemblies

Translational assemblies refer to an array of spatial scissor units that are linearly connected, as shown in Fig 2. Geometrically, the adjacent unit can be obtained through the transformation of translation of the first one. In this method, the two units are connected to each other with two end hubs. This type of assembly was proposed by Piñero in the 1960s [30], and several researchers have proposed designs to achieve different forms [12,33,48]. It should be noted that all of this literature focuses on a special configuration in which all the members are at the same deployment angle and all the joint axes are parallel to the same plane. In this way, the mechanism is axisymmetric throughout its transformation. There are two reasons why the previous research only studied this special configuration. Firstly, this configuration is the most commonly used form for

architectural purposes. The second reason is the lack of clarity about the mobility and motion modes of this system. Therefore, this study also starts with this configuration. On the one hand, to examine the instantaneous mobility of the assembly; on the other hand, to investigate all the possible configurations that can be obtained from this particular configuration. In order to study the mobility of a translational assembly using screw theory, we first review its geometric properties.

### 2.1 *Geometry of the translational assembly*

A single TSU consists of three identical members connecting by an intermediate hub. During the deployment, angle $\gamma$ is used to measure the members' rotation angle from the fully folded state, as shown in Fig 2a. In this study, the analysis focus on the configuration that all the members are rotated with the same angle $\gamma$. To connect one TSU to another, a top-end hub and a bottom-end hub are used. The translational assembly is a three-way linkage [36,49], in which adjacent TSUs are connected through a hinge at the top and another at the bottom. If only two units are assembled, one of the members in a TSU would become a "free member". Therefore, at least three units are required to form a basic translational assembly, i.e. all the three members can be connected to a member of another unit. The three-unit assembly can avoid the additional mobility caused by a "free member", which is not a part of any kinematic loops. In this assembly, the members and the joints can be divided into three families according to their orientation.

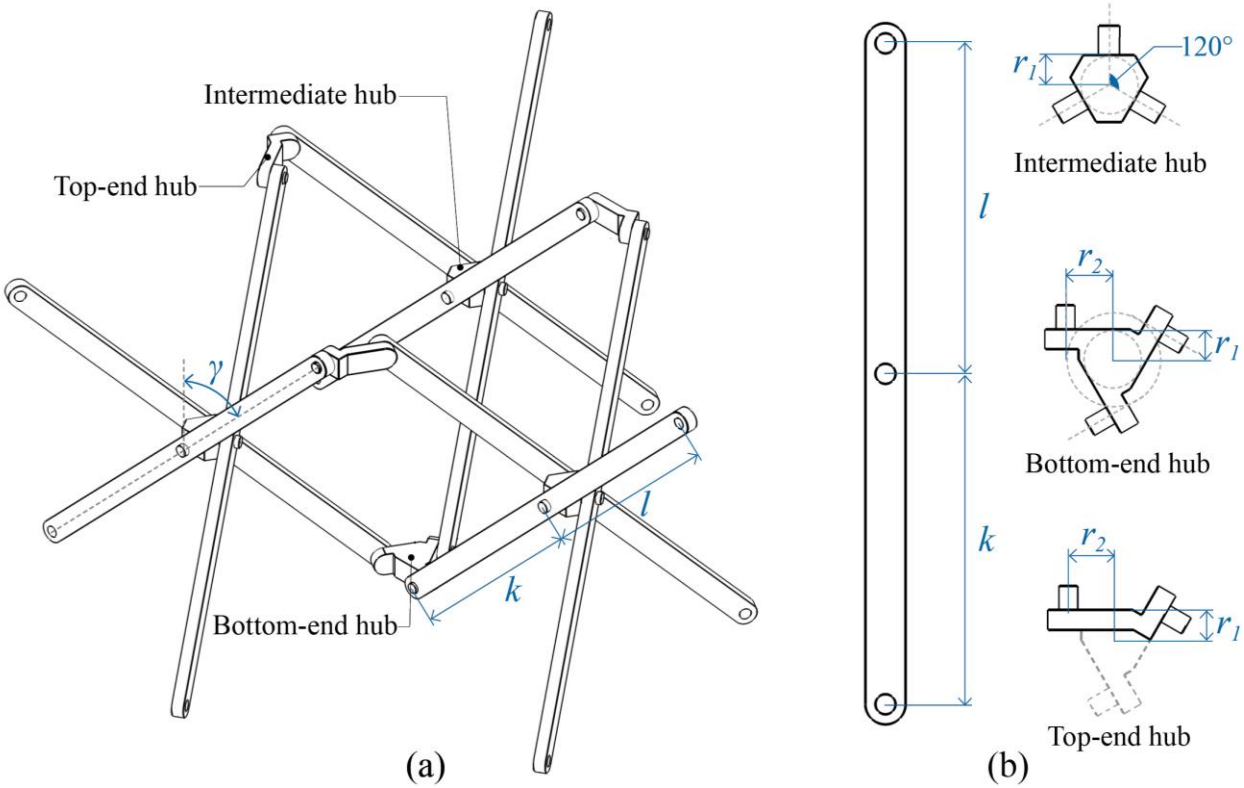


Figure 2. (a) A translational assembly made of three TSUs, and (b) the geometries of the components.

The geometries of all the components are illustrated in Fig. 2b. A member has three hinge holes, which divide the member's length into two segments. The semi-length of the upper segment is $l$ and the lower segment is $k$. The intermediate hub is connected to three members via revolute

joints. The internal part of a hub has a radius of $r_1$. The joint axes associated with a hub are coplanar and intersect at a common point with 120° between each pair of axes. The bottom-end hub also has three revolute joints with coplanar axes. However, the joint axes do not all intersect at a common point. The distance from the center to each joint axis is $r_2$, and the radius of the internal part must be equal to $r_1$. The top-end hub has two joints, which is can be considered as a part of the bottom-end joint when one joint axis is removed. So, they share similar geometries. To sum up, the translational assembly is made of four types of components: one type of members and three types of hubs. All the joints only allow the members to rotate freely about the joint axis of their connection but restrain all other DOFs.

It is worth noting that the design of components shown in Fig. 2 is only to demonstrate the kinematic characteristics of the proposed mechanism. As in the previous research [30,33,34,48,49], this system has been proven to be a feasible structural mechanism in the reciprocal state. Therefore, for structural purposes, members with circular cross sections and reasonable joint sizes are preferred to avoid crushing at contact points and offsets between members [50].

### *2.2 Mobility of translational assembly*

Straight scissor units made of members with unequal semi-length ($l \neq k$) are a more general situation. They are typically called polar units that are used to obtain curved forms. One example is the deployable roof structure designed by Piñero using spatial polar units [30]. In this study, $l$ denotes the upper segment's length and $k$ denotes the lower segment's length, as shown in Fig. 2.

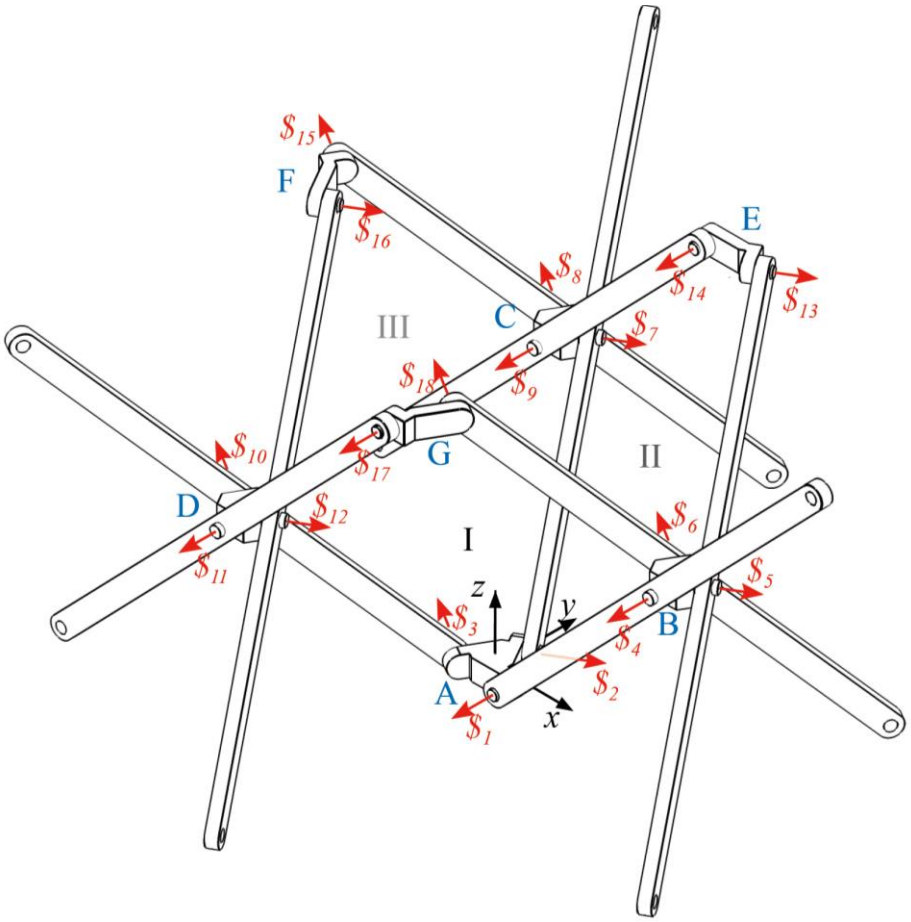

Figure 3. Screws of a translational assembly using TSUs.

For the assembly shown in Fig 3, hubs are labeled using a single uppercase letter, i.e. A, B, C… Members are named using the uppercase letters of the joints that they connect to, for example, AB denotes the member connecting to joints A and B. The rotational motions between members and hubs are expressed by a screw $\$_i$, for example, $\$_1$ denotes the rotation between joint A and member AB, as shown in Fig. 3. Since all joints are revolute joints, all screws are zero-pitch screws, i.e. lines.

The global coordinate system *A-xyz* is established with its origin at the center of hub A, as shown in Fig. 3. Axis *z* vertically points up; *x*-axis is perpendicular to *z*-axis and $\$_1$; *y*-axis follows the right-hand rule.

Assuming the angle between each member and *z*-axis is $\gamma$, with the components' geometries from section 2.1, the screw coordinates of each revolute joint can be written. Taking an example of $\$_1$, its axis vector $\boldsymbol{q}_1$ and arm vector $\boldsymbol{p}_1$ can be written as

$$\boldsymbol{q}_1 = \begin{pmatrix} 0 & -1 & 0 \end{pmatrix}^{\mathrm{T}} \tag{1}$$

$$\boldsymbol{p}_1 = \begin{pmatrix} r_2 & -r_1 & 0 \end{pmatrix}^{\mathrm{T}} \tag{2}$$

According to screw theory, the screw of revolute joint-1 can be expressed as

$$\$_1 = \begin{pmatrix} q_1 & p_1 \times q_1 \end{pmatrix}^{\mathrm{T}} = \begin{pmatrix} 0 & -1 & 0 & 0 & 0 & -r_2 \end{pmatrix}^{\mathrm{T}} \tag{3}$$

Following the same procedure, the screws of the remaining kinematic pairs can be obtained. $\$_1$-$\$_{18}$ are listed in Appendix A.

Based on graph theory, the assembly in Fig. 3 can be expressed using a topological diagram [51], which is given in Fig. 4. In the diagram, the nodes stand for the links, i.e. members and hubs. The edges connecting the nodes represent the joints.

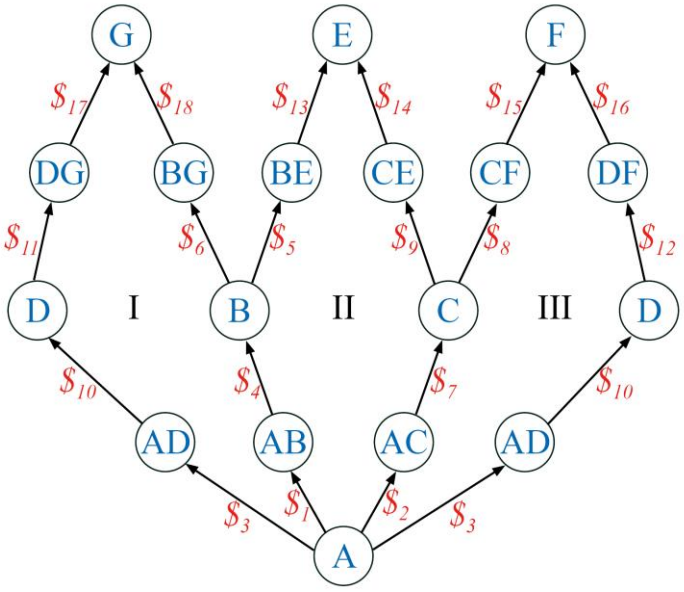


Figure 4. Topological diagram showing the constraints of a translational TSU assembly.

The topological diagram shows three loops (I, II, and III in Fig. 4), which can be selected as

the three independent loops. This is consistent with the result using Euler's formula: $n = q - p + 1$, which indicates, in a multi-loop linkage, the number of independent loops $n$ equals the number of joints $q$ minus the number links $p$ plus one.

Therefore, we can write the velocity loop equations for the assembly using the screws as

$$\begin{cases} -\omega_1\$_1 + \omega_3\$_3 - \omega_4\$_4 - \omega_6\$_6 + \omega_{10}\$_{10} + \omega_{11}\$_{11} + \omega_{17}\$_{17} - \omega_{18}\$_{18} = 0 \\ \omega_1\$_1 - \omega_2\$_2 + \omega_4\$_4 + \omega_5\$_5 - \omega_7\$_7 - \omega_9\$_9 + \omega_{13}\$_{13} - \omega_{14}\$_{14} = 0 \\ \omega_2\$_2 - \omega_3\$_3 + \omega_7\$_7 + \omega_8\$_8 - \omega_{10}\$_{10} - \omega_{12}\$_{12} + \omega_{15}\$_{15} - \omega_{16}\$_{16} = 0 \end{cases} \tag{4}$$

where $\omega_i$ denotes the angular speed of the $i^{\text{th}}$ revolute joint in the assembly. Eq. (4) can be rewritten in a matrix form as

$$\mathbf{S}_{\text{t}}\boldsymbol{\Omega}_{\text{t}} = \mathbf{0} \tag{5}$$

where

$$\mathbf{S}_{\text{t}} = \begin{bmatrix} -\$_1 & \mathbf{0} & \$_3 & -\$_4 & \mathbf{0} & -\$_6 & \mathbf{0} & \mathbf{0} & \mathbf{0} & \$_{10} & \$_{11} & \mathbf{0} & \mathbf{0} & \mathbf{0} & \mathbf{0} & \mathbf{0} & \$_{17} & -\$_{18} \\ \$_1 & -\$_2 & \mathbf{0} & \$_4 & \$_5 & \mathbf{0} & -\$_7 & \mathbf{0} & -\$_9 & \mathbf{0} & \mathbf{0} & \mathbf{0} & \$_{13} & -\$_{14} & \mathbf{0} & \mathbf{0} & \mathbf{0} & \mathbf{0} \\ \mathbf{0} & \$_2 & -\$_3 & \mathbf{0} & \mathbf{0} & \mathbf{0} & \$_7 & \$_8 & \mathbf{0} & -\$_{10} & \mathbf{0} & -\$_{12} & \mathbf{0} & \mathbf{0} & \$_{15} & -\$_{16} & \mathbf{0} & \mathbf{0} \end{bmatrix} \tag{6}$$

$$\boldsymbol{\Omega}_{\text{t}} = \begin{pmatrix} \omega_1 & \omega_2 & \omega_3 & \ldots & \omega_{18} \end{pmatrix}^{\text{T}} \tag{7}$$

and $\mathbf{0}$ in Eq. (5) is an 18×1 null column matrix. In Eq. (6), each screw $\$_i$ is a 6×1 column matrix, and each $\mathbf{0}$ is a 6×1 null column matrix. Therefore, the dimension of $\mathbf{S_t}$ is 18×18. Observing Eq. (5), it can be found that, since all joint axes are parallel to the *xy*-plane, the third entry of all screws are zero. So, third, ninth and fifteenth rows of $\mathbf{S_t}$ matrix are rows of zeroes, and maximum rank of $\mathbf{S_t}$ can be 15 and the DOF of the assembly would be 3 if there is no over-constraint in the 5-dimensional motion space (no link rotates about the *z*-axis). Indeed, if the Chebyshev-Grübler-Kutzbach (CGK) mobility would be used to evaluate the DOF of the mechanism with a 5-dimensional motion space, the result would be $M = 5 \times (16 - 18 - 1) + 18 = 3$ for 16 links and 18 revolute joints. According to [52], the mobility $M$ of a multi-loop assembly equals the number of columns that are linearly dependent in the matrix, i.e. the dimension of its null space, which can be expressed as

$$M = nullity\left(\mathbf{S}_{\mathbf{t}}\right) = Dimension\left(\mathbf{S}_{\mathbf{t}}\right) - Rank\left(\mathbf{S}_{\mathbf{t}}\right) \tag{8}$$

Computing the rank of $\mathbf{S_t}$ symbolically gives a result of 14. Thus, the translational assembly using unequal semi-length members has four DOFs ($M = 18 - 14 = 4$). There seems to be one degree of over-constraint, but this extra DOF could be an isolated (i.e. instantaneous) DOF as well. The CAD model simulations and prototype tests (see Section 4) show that all 4 DOFs are finite DOFs, but not all of them can be actuated simultaneously.

Solving Eq. (5), namely finding the null space of $\mathbf{S_t}$, gives four linearly independent solutions. These results can be expressed in a form of 18×1 column matrix $(\omega_1\ \omega_2\ \omega_3\ \ldots\ \omega_{18})^{\text{T}}$ as

$$\boldsymbol{\Omega}_{\text{t1}} = \begin{pmatrix} 1 & 0 & 0 & -1 & 0 & 0 & 0 & 0 & \dfrac{k}{l} & 0 & \dfrac{k}{l} & 0 & 0 & -\dfrac{k}{l} & 0 & 0 & -\dfrac{k}{l} & 0 \end{pmatrix}^{\text{T}} \tag{9.1}$$

$$\boldsymbol{\Omega}_{t2} = \begin{pmatrix} 0 & 1 & 0 & 0 & \frac{k}{l} & 0 & -1 & 0 & 0 & 0 & 0 & \frac{k}{l} & -\frac{k}{l} & 0 & 0 & -\frac{k}{l} & 0 & 0 \end{pmatrix}^{\mathrm{T}} \tag{9.2}$$

$$\boldsymbol{\Omega}_{t3} = \begin{pmatrix} 0 & 0 & 1 & 0 & 0 & \frac{k}{l} & 0 & \frac{k}{l} & 0 & -1 & 0 & 0 & 0 & 0 & -\frac{k}{l} & 0 & 0 & -\frac{k}{l} \end{pmatrix}^{\mathrm{T}} \tag{9.3}$$

$$\boldsymbol{\Omega}_{t4} = \begin{pmatrix} 0 & 0 & 0 & 1 & 1 & 1 & 1 & 1 & 1 & 1 & 1 & 1 & 0 & 0 & 0 & 0 & 0 & 0 \end{pmatrix}^{\mathrm{T}} \tag{9.4}$$

where each of them implies one DOF of the assembly. For instance, Eq. (9.1) represents the motion that when there is a unit angle rotation about ***$1*** in one sense, there will be a unit angle rotation about ***$4*** in the opposite sense; there will be *k*/*l* unit angle rotation about ***$9*** and ***$11*** in the same sense; and *k*/*l* unit angle rotation about ***$14*** and ***$17*** in the opposite sense; whereas all the rest of the joints remain immobile, as shown in Fig. 5a. In other words, only the joints, axes of which are in the same family move and the associated members rotate simultaneously for this case. However, ***$9*-*$11*** and ***$14*-*$17*** screw pairs are no longer coaxial during transformation, which result in a spatial loop link in the assembly. This may make the instantaneous DOF infinitesimal rather than a finite DOF, which requires further analysis in the future study.

Similarly for Eqs. (9.2) and (9.3), which represent the motion of the members in the other two families, the motions are shown in Fig. 5b and c. Therefore, we can conclude that components from each family have an independent instantaneous mobility and these three motion modes can be actuated simultaneously.

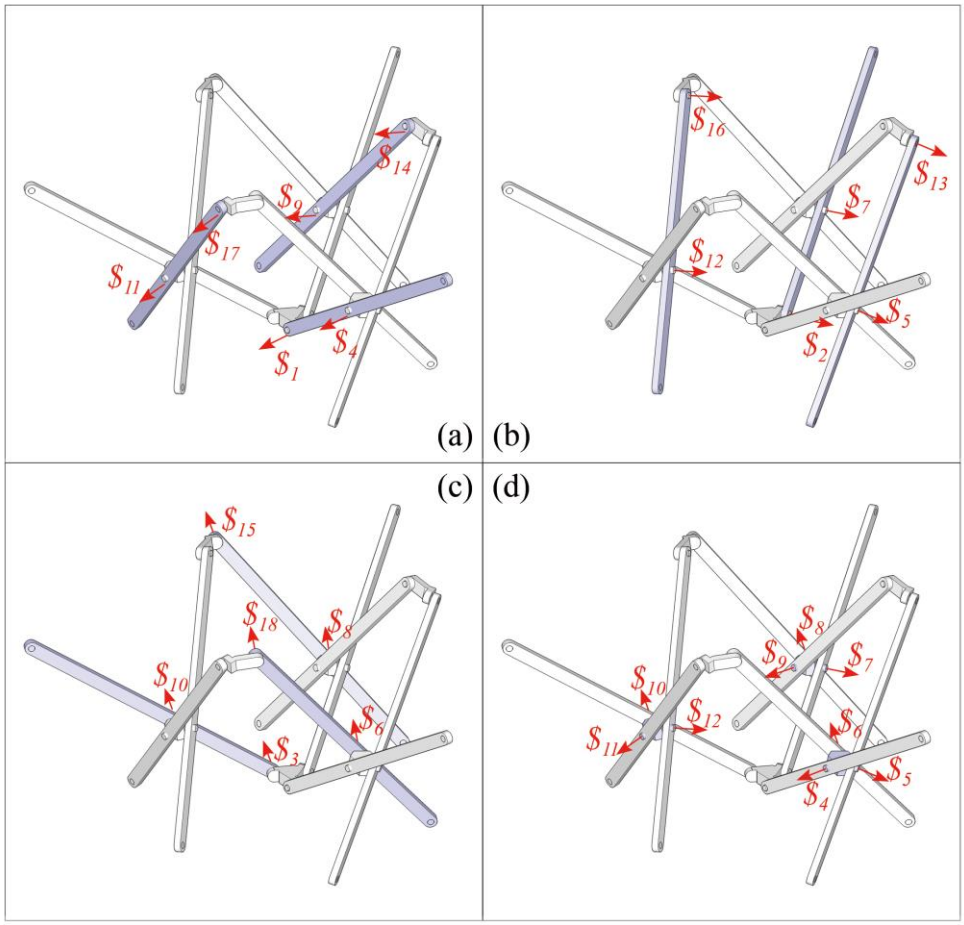

Figure 5. Active screws and components in the motion of a translational assembly using members with unequal segments: (a) first DOF, (b) second DOF, (c) third DOF, and (d) fourth DOF.

Eq. (9.4) shows a type of motion that has different characteristics than the other three DOFs. In this situation, $\$_4$-to-$\$_{12}$ rotate in the same sense by the same amount at the same time. It can be found from Fig. 5d that $\$_4$-to-$\$_{12}$ are all the screws of the intermediate hubs. Hence, this motion can be understood as all the intermediate joints rotate simultaneously, but the rest of the joints remain immobile such that the bottom and upper hubs are as if rigidly connected to the links joined to them This 4th DOF is verified with computer simulations and prototypes. In this mode, the top and intermediate hubs do not remain parallel to the bottom hub (i.e. their joint axes are not coplanar). However, the range of motion is very limited. When we look at the loops (for instance loop $\$_5$-$\$_6$-$\$_7$-$\$_8$), they are 4-bar loops. It is very well known that the only mobile 4-bar loops are the planar 4-bar, the spherical 4-bar and the Bennett 4-bar. Since the 4-bar loop in consideration comprises 3 universal joints ($\$_5$-$\$_6$ and $\$_7$-$\$_8$ pairs intersect), is cannot be a finitely mobile loop. Therefore, we conclude that this is not a finite DOF, but an infinitesimal DOF, i.e. the mechanism is shaky [53,54].

Planar scissor units made of members with equal semi-length are a special case when $l = k$. They are also called translational units, as they usually lead to linear transformation [55]. Thus, we can use a single parameter $l$ to indicate the length of both segments.

Using the same reference frame and the same geometric parameters (except for $l$ and $k$) from Fig. 3, we can find the screws $\$'_i$ of the assembly using members with equal semi-length. $\$'_1$-$\$'_3$ are the same as $\$_1$-$\$_3$, but $\$'_4$-$\$'_{18}$ are different due to the change of the member's length. $\$'_1$-$\$'_{18}$ are given in Appendix B.

Substituting $\$'_1$-$\$'_{18}$ into Eqs. (4)-(8), we can write $\mathbf{S'_t}$ and $\mathbf{\Omega'_t}$ following the same procedure. Consequently, it can be found that the mobility of a translational assembly using equal semi-length members is also four DOFs. And calculating the null space of $\mathbf{S'_t}$ gives four linearly independent solutions as

$$\mathbf{\Omega}'_{t1} = \begin{pmatrix} -1 & 0 & 0 & 1 & 0 & 0 & 0 & 0 & -1 & 0 & -1 & 0 & 0 & 1 & 0 & 0 & 1 & 0 \end{pmatrix}^{\mathrm{T}} \tag{10.1}$$

$$\mathbf{\Omega}'_{t2} = \begin{pmatrix} 0 & -1 & 0 & 0 & -1 & 0 & 1 & 0 & 0 & 0 & 0 & -1 & 1 & 0 & 0 & 1 & 0 & 0 \end{pmatrix}^{\mathrm{T}} \tag{10.2}$$

$$\mathbf{\Omega}'_{t3} = \begin{pmatrix} 0 & 0 & -1 & 0 & 0 & -1 & 0 & -1 & 0 & 1 & 0 & 0 & 0 & 0 & 1 & 0 & 0 & 1 \end{pmatrix}^{\mathrm{T}} \tag{10.3}$$

$$\mathbf{\Omega}'_{t4} = \begin{pmatrix} 0 & 0 & 0 & 1 & 1 & 1 & 1 & 1 & 1 & 1 & 1 & 1 & 0 & 0 & 0 & 0 & 0 & 0 \end{pmatrix}^{\mathrm{T}} \tag{10.4}$$

Eqs. (10.1)-(10.4) show that the assembly using equal semi-length members has similar motion types, i.e. each family of members has an independent DOF, and the intermediate hubs have the fourth DOF. However, due to the equal semi-length of the members, $\$'_9$-$\$'_{11}$ and $\$'_{14}$-$\$'_{17}$ screw pairs remain coaxial, and the parallel links in between these joints move together as if they are the same link, as shown in Fig. 6a. In this mode, the mechanism reduces merely to a planar 4-bar linkage (with link length proportions of a parallelogram loop). This results in finite DOFs for the first three motion modes, as shown in Fig. 6a-c. Also, the resulting motion of the unit will be different, which is known as a linear motion. However, the last motion mode, as shown in Fig. 6d, is still an infinitesimal DOF due to the same reason for the general case. Therefore, for the translational assembly with equilateral members, we conclude that the mechanism has 3 finite

DOFs and 1 infinitesimal DOF at the selected type of configurations, i.e. when all members have the identical deployment angle.

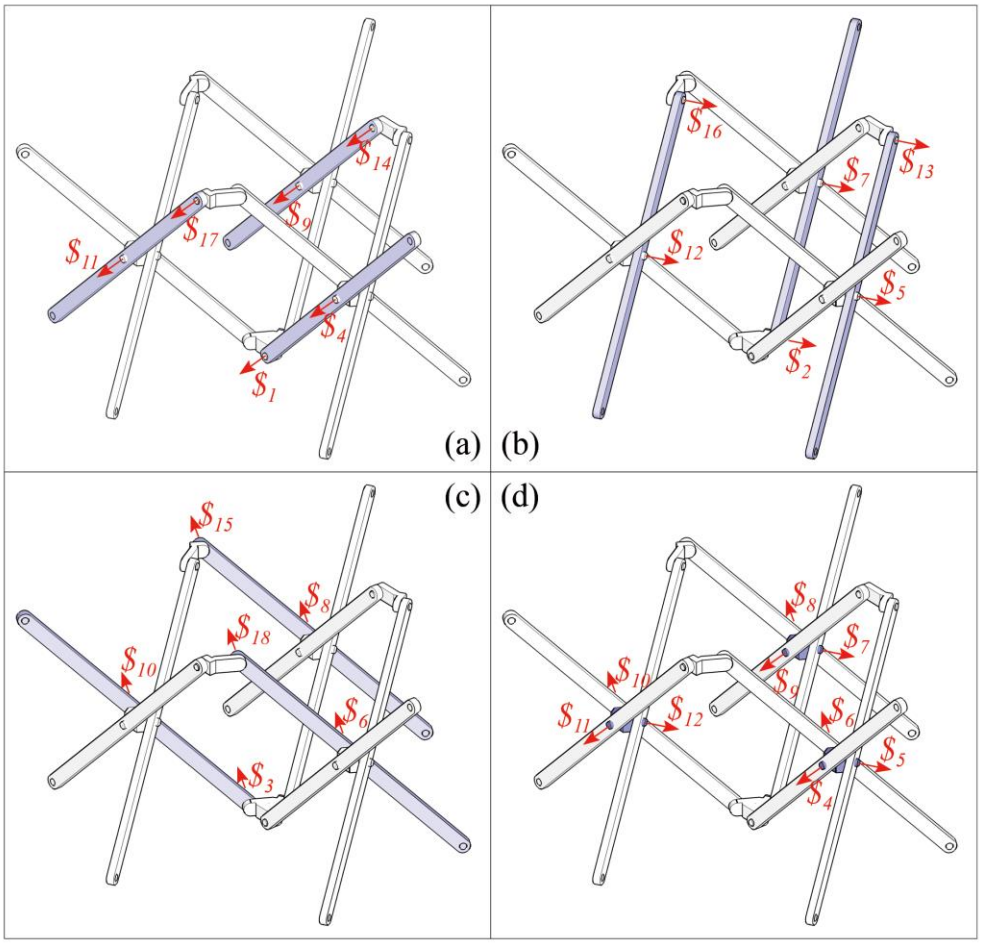


Figure 6. Active screws and components in the motion of a translational assembly with equilateral members: (a) first DOF, (b) second DOF, (c) third DOF, and (d) fourth DOF.

To sum up, we can conclude that the translational assemblies, in the configuration when all the members are unfolded with an identical angle, have four instantaneous DOFs, no matter using equal or unequal semi-length members. In addition, it can be observed that, as long as members are identical, the change in the member's segmental length does not influence the instantaneous mobility of the system. But it may make a difference of whether the first three DOFs are infinitesimal or finite.

## 3. Mobility analysis of mirrored assemblies

Mirrored TSU structures were proposed by Liao and Krishnan using a different assembly approach [36]. They are named as mirrored assemblies because, if ignoring the link thicknesses, the circumjacent units are mirror symmetric with respect to the central unit about the plane defined by their connecting points, as shown in Fig 7a. Therefore, the adjacent unit can be obtained through a reflection. In this type of assembly, units are connected at three locations, and different joints are required as shown in Fig. 7. For comparison with the translational assemblies, we use a simple mirrored assembly here to analyze its mobility. Its geometric design of long-span structures, such

as domes and polyhedral forms, have been presented in [36,37]. The geometry of the basic mirrored assembly is reviewed below in preparation for the mobility analysis.

### 3.1 *Geometry of the mirrored assembly*

In a physical mirrored TSU model, the thicknesses of members and hubs cause offsets between units, so they are not simply mirror symmetric. There are two ways to obtain a circumjacent unit. The first way is to mirror the central unit twice about different planes of symmetry. Firstly, reflecting the central unit about the symmetry plane defined by the end points of the theoretical member lines (the red dashed lines in Fig. 7a). The theoretical member line is the situation where all the members and joints have zero thickness, where three member lines with segmental lengths of $l$ and $k$ will intersect at the same point. Secondly, reflecting the unit about the vertical plane passing through its bottom-end joint. The second step is to overcome the transverse offsets between two units.

The other way is to replace the two reflections with a rotation. To obtain a circumjacent unit, we can rotate the central unit 180° about the axis on the symmetry plane (the green line in Fig. 7). This method can simplify the transformation matrices in computation, so it is used to find the screws for the mirrored assembly in the following procedure.

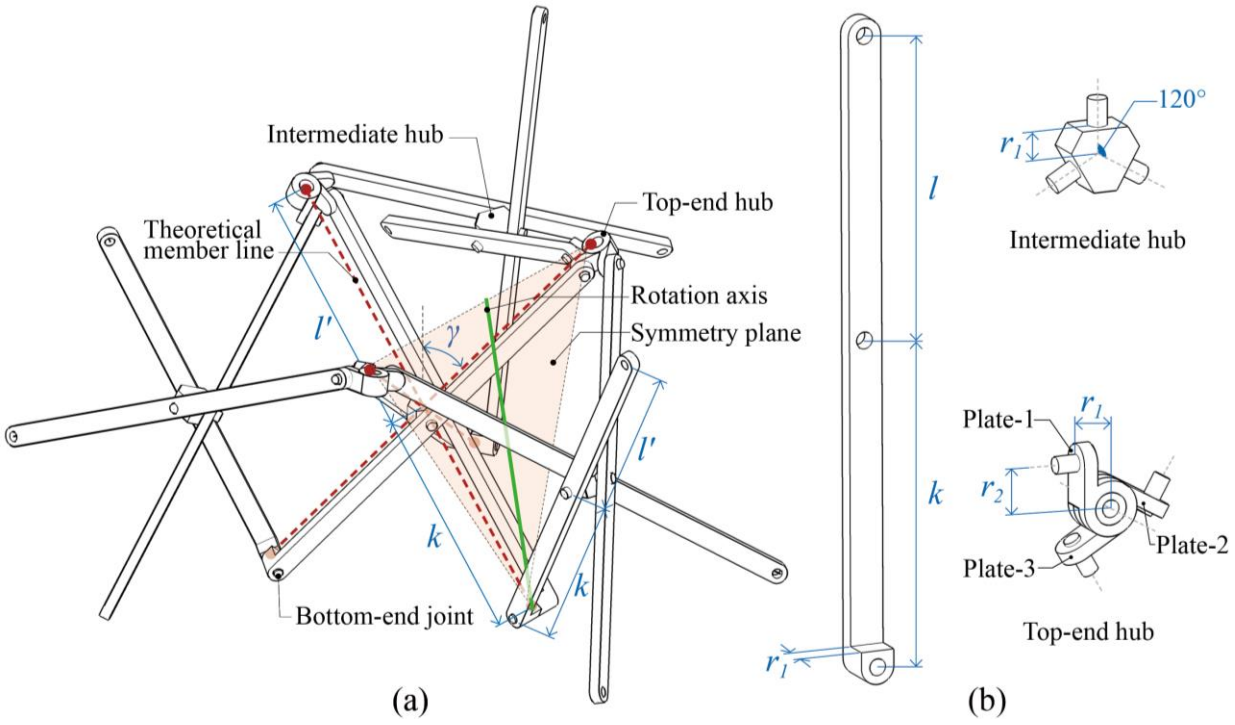


Figure 7. (a) A mirrored assembly made of four TSUs, and (b) the geometries of the components.

The hubs used to connect the units are different from the translational assemblies. The top-end hub has three extension plates that can rotate around a central axis, and each plate connects to a member via a revolute joint. The dimensions are given in Fig. 7b. There is no hub at the bottom, but the members are simply connected with a revolute joint.

Observing Fig. 7a, it can be found that (1) the intermediate hub creates transverse offsets, (2) the top-end hub generates both transverse and longitudinal offsets, and (3) the bottom-end joint does not cause any offset. Therefore, the member shape should be modified to accommodate all

the offsets caused by each type of joints. For the upper segment, its length should be shortened as

$$l = l' - \frac{r_2(2k - l')}{2\sqrt{2}k}\sqrt{1 + \frac{8(k + l')^2}{(2k - l')^2}} \tag{11}$$

where $l$ is the shortened upper segmental length and $l'$ is the theoretical upper segmental length that is used to define the symmetry between the units. The derivation of Eq. (11) is given in Appendix C. For the lower segment, the members are modeled to have an L-shape at the bottom connections in Fig. 2. However, to ease the fabrication, we can keep the members straight but add a washer in between the members to overcome the transverse offsets of $2r_1$.

### *3.2 Mobility of mirrored assembly*

We first analyze the mobility of a mirrored assembly in general cases, i.e. members with unequal semi-length ($k \neq l'$). Similarly, $k$ denotes the lower segment's length and $l'$ denotes the theoretical upper segment's length, as shown in Fig. 8. Following the same way to label the links and joints, the screws are marked in Fig. 8. The global coordinate system $A'$-$xyz$ is established with its origin at the center of hub A, where $z$-axis vertically points up; $y$-axis is along $\$_m^1$; $x$-axis follows the right-hand rule.

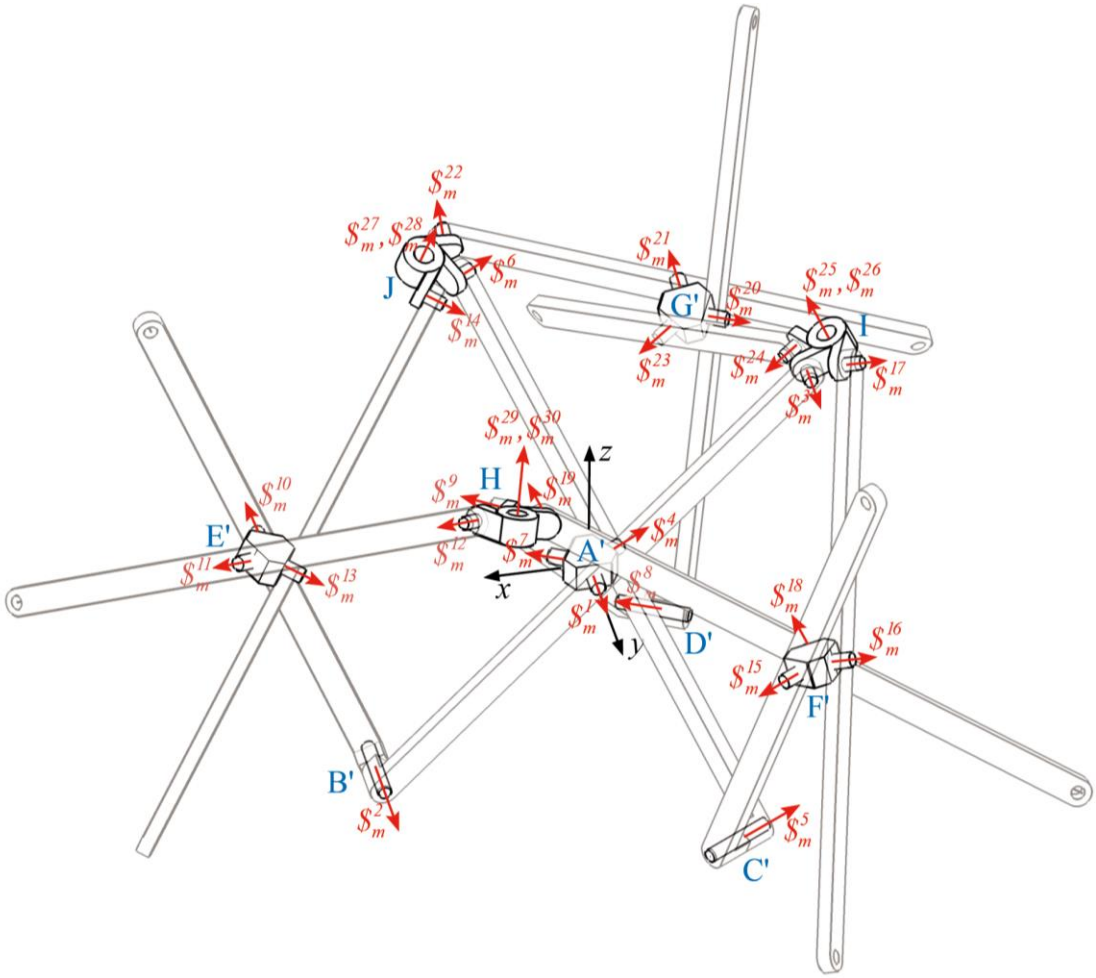


Figure 8. Screws of a mirrored assembly using TSUs.

Writing the screws can start from a member in the central unit. For example, $\$_m^1$ - $\$_m^3$ are perpendicular to the *xz*-plane, which can be obtained using their unit orientation vectors $\boldsymbol{q}_m^1$ - $\boldsymbol{q}_m^3$ and arm vectors $\boldsymbol{p}_m^1$ - $\boldsymbol{p}_m^3$:

$$\boldsymbol{q}_m^1 = \begin{pmatrix} 0 & 1 & 0 \end{pmatrix}^{\mathrm{T}}, \boldsymbol{p}_m^1 = \begin{pmatrix} 0 & r_1 & 0 \end{pmatrix}^{\mathrm{T}}, \$_m^1 = \begin{pmatrix} \boldsymbol{q}_m^1 & \boldsymbol{p}_m^1 \times \boldsymbol{q}_m^1 \end{pmatrix}^{\mathrm{T}} \tag{12.1}$$

$$\boldsymbol{q}_m^2 = \boldsymbol{q}_m^1, \boldsymbol{p}_m^2 = \begin{pmatrix} k\sin\gamma & 0 & -k\cos\gamma \end{pmatrix}^{\mathrm{T}}, \$_m^2 = \begin{pmatrix} \boldsymbol{q}_m^2 & \boldsymbol{p}_m^2 \times \boldsymbol{q}_m^2 \end{pmatrix}^{\mathrm{T}} \tag{12.2}$$

$$\boldsymbol{q}_m^3 = \boldsymbol{q}_m^1, \boldsymbol{p}_m^3 = \begin{pmatrix} -l\sin\gamma & 0 & l\cos\gamma \end{pmatrix}^{\mathrm{T}}, \$_m^3 = \begin{pmatrix} \boldsymbol{q}_m^3 & \boldsymbol{p}_m^3 \times \boldsymbol{q}_m^3 \end{pmatrix}^{\mathrm{T}} \tag{12.3}$$

where $\gamma$ is the rotation angle of a member from the fully folded state. Assuming $\gamma$ is identical for all the members. Other screws in the central unit can be written using rotations. For example, $\$_m^4$ can be expressed as

$$\$_m^4 = \begin{pmatrix} \mathbf{R}\boldsymbol{q}_m^1 & \left(\mathbf{R}\boldsymbol{p}_m^1\right) \times \left(\mathbf{R}\boldsymbol{q}_m^1\right) \end{pmatrix}^{\mathrm{T}} \tag{13}$$

where **R** is the rotation matrix about the z-axis by 120°:

$$\mathbf{R} = \begin{bmatrix} \cos(2\pi/3) & -\sin(2\pi/3) & 0 \\ \sin(2\pi/3) & \cos(2\pi/3) & 0 \\ 0 & 0 & 1 \end{bmatrix} \tag{14}$$

The screws of the circumjacent units can be obtained using rotation about the axis on the plane of symmetry. For example, $\$_m^{10}$ can be written as

$$\$_m^{10} = \begin{pmatrix} \mathbf{R}_1\boldsymbol{q}_m^1 & \left(\mathbf{R}_1\boldsymbol{p}_m^1 + \mathbf{T}_1\right) \times \left(\mathbf{R}_1\boldsymbol{q}_m^1\right) \end{pmatrix}^{\mathrm{T}} \tag{15}$$

where $\mathbf{R_1}$ and $\mathbf{T_1}$ are the transformation matrices

$$\mathbf{R}_1 = \begin{bmatrix} \dfrac{(2k-l')^2\tan^2\gamma - 4(k+l')^2}{(2k-l')^2\tan^2\gamma + 4(k+l')^2} & 0 & \dfrac{-4(2k-l')(k+l')\tan\gamma}{(2k-l')^2\tan^2\gamma + 4(k+l')^2} \\ 0 & -1 & 0 \\ \dfrac{4(2k-l')(k+l')\tan\gamma}{(2k-l')^2\tan^2\gamma + 4(k+l')^2} & 0 & -\dfrac{(2k-l')^2\tan^2\gamma - 4(k+l')^2}{(2k-l')^2\tan^2\gamma + 4(k+l')^2} \end{bmatrix} \tag{16.1}$$

$$\mathbf{T}_1 = \begin{bmatrix} \dfrac{12kl'(k+l')\sin\gamma}{(2k-l')^2\tan^2\gamma + 4(k+l')^2} & 0 & \dfrac{6kl'(2k-l')\tan\gamma\sin\gamma}{(2k-l')^2\tan^2\gamma + 4(k+l')^2} \end{bmatrix}^T \tag{16.2}$$

Similarly, the screws of the remaining revolute joints can be obtained. $\$_m^1$-$\$_m^{30}$ are listed in Appendix D.

The topological diagram of the mirrored assembly is given in Fig. 9 based on graph theory. It should be noted that the top-end hubs H, I, and J have three extension plates connecting at their central hinge, which are labeled as -1, -2, and -3, respectively. Therefore, two screws coincide along the central axis of each top-end joint, such as $\$_m^{25}$ and $\$_m^{26}$.

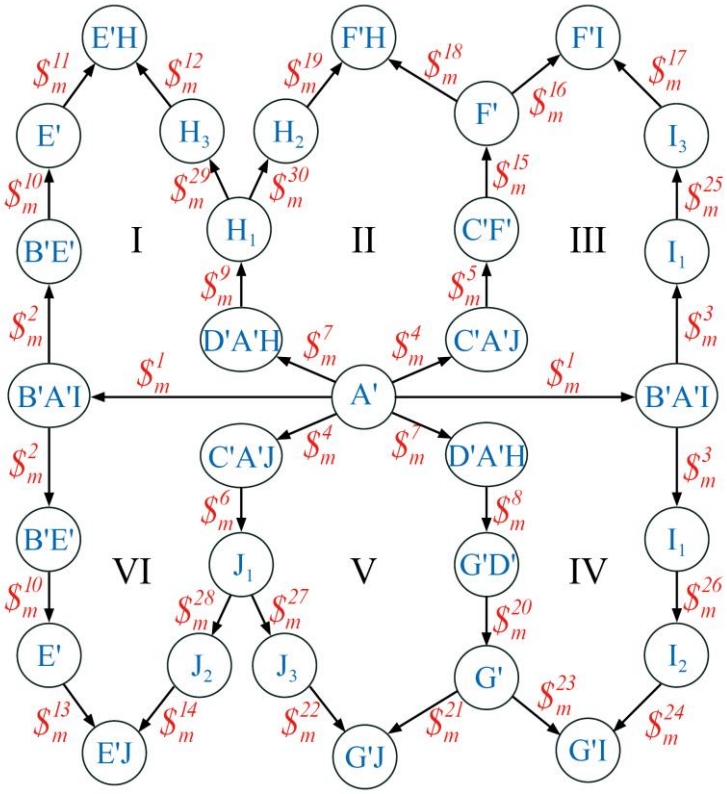


Figure 9. Topological diagram showing the constraints of the mirrored TSU assembly.

The topological diagram has six independent loops. Using Euler's formula: $n = q - p + 1$, we can get the same result (30 – 25 + 1 = 6). In this case, the loop closure equations for this assembly are given by

$$\begin{cases} \omega_m^1 \$_m^1 + \omega_m^2 \$_m^2 - \omega_m^7 \$_m^7 - \omega_m^7 \$_m^7 + \omega_m^{10} \$_m^{10} + \omega_m^{11} \$_m^{11} - \omega_m^{12} \$_m^{12} - \omega_m^{29} \$_m^{29} = 0 \\ -\omega_m^4 \$_m^4 - \omega_m^5 \$_m^5 + \omega_m^7 \$_m^7 + \omega_m^9 \$_m^9 - \omega_m^{15} \$_m^{15} - \omega_m^{18} \$_m^{18} + \omega_m^{19} \$_m^{19} + \omega_m^{30} \$_m^{30} = 0 \\ -\omega_m^1 \$_m^1 - \omega_m^3 \$_m^3 + \omega_m^4 \$_m^4 + \omega_m^5 \$_m^5 + \omega_m^{15} \$_m^{15} + \omega_m^{16} \$_m^{16} - \omega_m^{17} \$_m^{17} - \omega_m^{25} \$_m^{25} = 0 \\ \omega_m^1 \$_m^1 + \omega_m^3 \$_m^3 - \omega_m^7 \$_m^7 - \omega_m^8 \$_m^8 - \omega_m^{20} \$_m^{20} - \omega_m^{23} \$_m^{23} + \omega_m^{24} \$_m^{24} + \omega_m^{26} \$_m^{26} = 0 \\ -\omega_m^4 \$_m^4 - \omega_m^6 \$_m^6 + \omega_m^7 \$_m^7 + \omega_m^8 \$_m^8 + \omega_m^{20} \$_m^{20} + \omega_m^{21} \$_m^{21} - \omega_m^{22} \$_m^{22} - \omega_m^{27} \$_m^{27} = 0 \\ -\omega_m^1 \$_m^1 - \omega_m^2 \$_m^2 + \omega_m^4 \$_m^4 + \omega_m^6 \$_m^6 - \omega_m^{10} \$_m^{10} - \omega_m^{13} \$_m^{13} + \omega_m^{14} \$_m^{14} + \omega_m^{28} \$_m^{28} = 0 \end{cases} \tag{17}$$

where $\omega_m^i$ denotes the angular speed of the $i^{\text{th}}$ revolute joint in the mirrored assembly. Eq. (17) can be rewritten into a matrix form as

$$\mathbf{S}_{\mathrm{m}} \boldsymbol{\Omega}_{\mathrm{m}} = \mathbf{0} \tag{18}$$

where $\mathbf{0}$ is a 30×1 null column matrix, and

$$\mathbf{S}_{\mathbf{m}} = \begin{bmatrix} \mathbf{S}_{\mathbf{m}}^{\mathbf{1}} & \mathbf{S}_{\mathbf{m}}^{\mathbf{3}} & \mathbf{S}_{\mathbf{m}}^{\mathbf{5}} & \mathbf{S}_{\mathbf{m}}^{\mathbf{7}} & \mathbf{S}_{\mathbf{m}}^{\mathbf{9}} & \mathbf{S}_{\mathbf{m}}^{\mathbf{11}} \\ \mathbf{S}_{\mathbf{m}}^{\mathbf{2}} & \mathbf{S}_{\mathbf{m}}^{\mathbf{4}} & \mathbf{S}_{\mathbf{m}}^{\mathbf{6}} & \mathbf{S}_{\mathbf{m}}^{\mathbf{8}} & \mathbf{S}_{\mathbf{m}}^{\mathbf{10}} & \mathbf{S}_{\mathbf{m}}^{\mathbf{12}} \end{bmatrix}^{\mathrm{T}} \tag{19}$$

$$\boldsymbol{\Omega}_{\mathrm{m}} = \begin{pmatrix} \omega_m^1 & \omega_m^2 & \omega_m^3 & \ldots & \omega_m^{30} \end{pmatrix}^{\mathrm{T}} \tag{20}$$

where in Eq. (19), $\mathbf{S}_{\mathbf{m}}^{\mathbf{i}}$ is the $i^{\text{th}}$ submatrix in matrix $\mathbf{S_m}$, which is given by

$$\mathbf{S}_{\mathbf{m}}^{\mathbf{1}} = \begin{pmatrix} \$_m^1 & \$_m^2 & 0 & 0 & 0 & 0 & -\$_m^7 & 0 & \$_m^9 & \$_m^{10} & \$_m^{11} & -\$_m^{12} & 0 & 0 & 0 \end{pmatrix} \tag{21.1}$$

$$\mathbf{S}_{\mathbf{m}}^{\mathbf{2}} = \begin{pmatrix} 0 & 0 & 0 & 0 & 0 & 0 & 0 & 0 & 0 & 0 & 0 & 0 & 0 & \$_m^{29} & 0 \end{pmatrix} \tag{21.2}$$

$$\mathbf{S}_{\mathbf{m}}^{\mathbf{3}} = \begin{pmatrix} 0 & 0 & 0 & -\$_m^4 & -\$_m^5 & 0 & \$_m^7 & 0 & \$_m^9 & 0 & 0 & 0 & 0 & 0 & -\$_m^{15} \end{pmatrix} \tag{21.3}$$

$$\mathbf{S}_{\mathbf{m}}^{\mathbf{4}} = \begin{pmatrix} 0 & 0 & -\$_m^{18} & \$_m^{19} & 0 & 0 & 0 & 0 & 0 & 0 & 0 & 0 & 0 & 0 & \$_m^{30} \end{pmatrix} \tag{21.4}$$

$$\mathbf{S}_{\mathbf{m}}^{\mathbf{5}} = \begin{pmatrix} -\$_m^1 & 0 & -\$_m^3 & \$_m^4 & \$_m^5 & 0 & 0 & 0 & 0 & 0 & 0 & 0 & 0 & 0 & \$_m^{15} \end{pmatrix} \tag{21.5}$$

$$\mathbf{S}_{\mathbf{m}}^{\mathbf{6}} = \begin{pmatrix} \$_m^{16} & -\$_m^{17} & 0 & 0 & 0 & 0 & 0 & 0 & 0 & -\$_m^{25} & 0 & 0 & 0 & 0 & 0 \end{pmatrix} \tag{21.6}$$

$$\mathbf{S}_{\mathbf{m}}^{\mathbf{7}} = \begin{pmatrix} \$_m^1 & 0 & \$_m^3 & 0 & 0 & 0 & -\$_m^7 & -\$_m^8 & 0 & 0 & 0 & 0 & 0 & 0 & 0 \end{pmatrix} \tag{21.7}$$

$$\mathbf{S}_{\mathbf{m}}^{\mathbf{8}} = \begin{pmatrix} 0 & 0 & 0 & 0 & -\$_m^{20} & 0 & 0 & -\$_m^{23} & \$_m^{24} & 0 & \$_m^{26} & 0 & 0 & 0 & 0 \end{pmatrix} \tag{21.8}$$

$$\mathbf{S}_{\mathbf{m}}^{\mathbf{9}} = \begin{pmatrix} 0 & 0 & 0 & -\$_m^4 & 0 & -\$_m^6 & \$_m^7 & \$_m^8 & 0 & 0 & 0 & 0 & 0 & 0 & 0 \end{pmatrix} \tag{21.9}$$

$$\mathbf{S}_{\mathbf{m}}^{\mathbf{10}} = \begin{pmatrix} 0 & 0 & 0 & 0 & \$_m^{20} & \$_m^{21} & -\$_m^{22} & 0 & 0 & 0 & 0 & -\$_m^{27} & 0 & 0 & 0 \end{pmatrix} \tag{21.10}$$

$$\mathbf{S}_{\mathbf{m}}^{\mathbf{11}} = \begin{pmatrix} -\$_m^1 & -\$_m^2 & 0 & \$_m^4 & 0 & \$_m^6 & 0 & 0 & 0 & -\$_m^{10} & 0 & 0 & -\$_m^{13} & \$_m^{14} & 0 \end{pmatrix} \tag{21.11}$$

$$\mathbf{S}_{\mathbf{m}}^{\mathbf{12}} = \begin{pmatrix} 0 & 0 & 0 & 0 & 0 & 0 & 0 & 0 & 0 & 0 & 0 & 0 & \$_m^{28} & 0 & 0 \end{pmatrix} \tag{21.12}$$

In Eqs. (21), each screw $\$_m^i$ is a 6×1 column matrix, and each $\mathbf{0}$ is a 6×1 null column matrix. Therefore, the dimension of $\mathbf{S_m}$ is 36×30. Calculating the rank of $\mathbf{S_m}$ gives a result of 29. And using Eq. (8), the instantaneous mobility $M$ of a mirrored assembly equals one DOF ($M = 30 - 29 = 1$). The CGK formula would evaluate $M = 6 \times (25 - 30 - 1) + 30 = -6$ for 25 links and 30 revolute joints, so the degree of over-constraint of this mechanism is 7.

Solving Eq. (18) gives the null space of $\mathbf{S_m}$, which has only one independent solution. The nonlinear motion results in a very complex symbolic expression for the null space. Thus, we use a numerical computation with $k = 15$, $l' = 20$, $r_1 = 1$, $r_2 = 2$, and $\gamma = 30°$, and normalize the array by dividing all terms to its first entry. The result can be expressed in the form of a 30×1 column matrix $(\omega_1\ \omega_2\ \omega_3\ \ldots\ \omega_{30})^{\mathrm{T}}$ as

$$\begin{aligned} \mathbf{\Omega}_{\mathrm{m}} = \big(&1 \quad -1.43 \quad -1.55 \quad 1 \quad -1.43 \quad -1.55 \quad 1 \quad -1.43 \quad -1.55 \quad -1 \quad 1 \quad 1.55 \quad 1 \quad 1.55 \quad -1... \\ &...1 \quad 1.55 \quad 1 \quad 1.55 \quad -1 \quad 1 \quad 1.55 \quad 1 \quad 1.55 \quad -0.013 \quad 0.013 \quad -0.013 \quad 0.013 \quad -0.013 \quad 0.013\big)^{T} \end{aligned} \tag{22}$$

The special case should also be examined, when the mirrored assemblies are made of members with equal segmental lengths ($k = l'$). Similarly, $l$ denotes the upper segment's length and $k$ denotes the lower segment's length, as shown in Fig. 7. Using the same reference frame in Fig. 8 and considering the change of segmental lengths, we can write the screws $'\$_m^i$ of the mirrored assembly. Observing Fig. 8, we can find that only Eq. (12.2) needs to be rewritten as

$$'\$_m^2 = \begin{pmatrix} \mathbf{q}_m^2 & '\mathbf{p}_m^2 \times \mathbf{q}_m^2 \end{pmatrix}^{\mathrm{T}} \tag{23.1}$$

$$'\$_m^{25} = \begin{pmatrix} 'q_m^{25} & 'p_m^{25} \times 'q_m^{25} \end{pmatrix}^{\mathrm{T}} \tag{23.2}$$

where

$$'\mathbf{p}_m^2 = \begin{pmatrix} l' \sin\gamma & 0 & -l' \cos\gamma \end{pmatrix}^{\mathrm{T}} \tag{24.1}$$

$$'\boldsymbol{q}_m^{25} = \begin{pmatrix} 1 & 0 & \dfrac{(k+l')\cot\gamma}{2k-l'} \end{pmatrix}^{\mathrm{T}} \tag{24.2}$$

$$'\boldsymbol{p}_m^{25} = \begin{pmatrix} -l\sin\gamma - \dfrac{r_2(l'+k)\cot\gamma}{\sqrt{(2k-l')^2+\left((l'+k)\cot\gamma\right)^2}} & 0 & l\cos\gamma + \dfrac{r_2(2k-l')}{\sqrt{(2k-l')^2+\left((l'+k)\cot\gamma\right)^2}} \end{pmatrix}^{\mathrm{T}} \tag{24.3}$$

For the transformation matrices, Eqs. (16.1) and (16.2) can be simplified as

$$\mathbf{R}_1' = \begin{bmatrix} \dfrac{1-17\cos^2\gamma}{1+15\cos^2\gamma} & 0 & -\dfrac{4\sin 2\gamma}{1+15\cos^2\gamma} \\ 0 & -1 & 0 \\ -\dfrac{4\sin 2\gamma}{1+15\cos^2\gamma} & 0 & -\dfrac{1-17\cos^2\gamma}{1+15\cos^2\gamma} \end{bmatrix} \tag{25.1}$$

$$\mathbf{T}_1' = \begin{bmatrix} \dfrac{12l\cos\gamma\sin 2\gamma}{1+15\cos^2\gamma} & 0 & \dfrac{3l\sin\gamma\sin 2\gamma}{1+15\cos^2\gamma} \end{bmatrix}^{\mathrm{T}} \tag{25.2}$$

Substituting the rewritten Eqs. (23.1)-(25.2) into Eqs. (17)-(20), we can obtain $\mathbf{S'_m}$ and $\mathbf{\Omega'_m}$ for the mirrored assembly using polar units. Consequently, it can be found that the instantaneous mobility of a mirrored assembly using unequal semi-length members is also a single DOF.

Therefore, the mirrored assemblies using both equal and unequal semi-length members have one DOF. And, if identical members are used, the change in the member's segmental length does not influence the instantaneous mobility of the system.

## 4. Validation using physical models

Physical prototypes of tripod scissor assemblies are constructed to verify the results of mobility analyses from previous Sections. In the physical model, the bars are laser cut using white acrylic boards, and the joints are 3D printed using grey plastic filament, as shown in Figs. 10-12.

### *4.1 Prototype of the translational assembly*

The physical prototypes of translational assembly, using members with unequal (Fig. 10) and equal segments (Fig. 11) are able to achieve four motion branches. This is consistent with the analytical results using screw theory from Section 2. The red arrows represent the positions and directions where we add force to fold the assembly. Observing the first three DOFs, it can be found that they share the same motion type, just along three different directions of the tripod form. In addition, these three motion modes can be combined together to achieve partially or completely folded configurations, and vice versa for its deployment process.

However, the 4$^{th}$ DOF cannot be combined with the first three DOFs. This can be observed from Fig. 10 that, in the 4$^{th}$ DOF, the top and intermediate hubs do not remain parallel to the bottom, and the range of motion is very limited. This implies that geometric incompatibility occurs during this transformation. The simulations with APEX software that considered elastic deformations validated this behavior, as shown in the supplementary video. Namely, the fourth DOF is just instantaneous mobility that exists in the configuration when all the members are rotated with an identical angle from the folded state. But this DOF still needs to receive enough attention in the design, because the relatively small geometric incompatibility would allow considerable non-

stress-free motion in reality, due to the material elasticity.

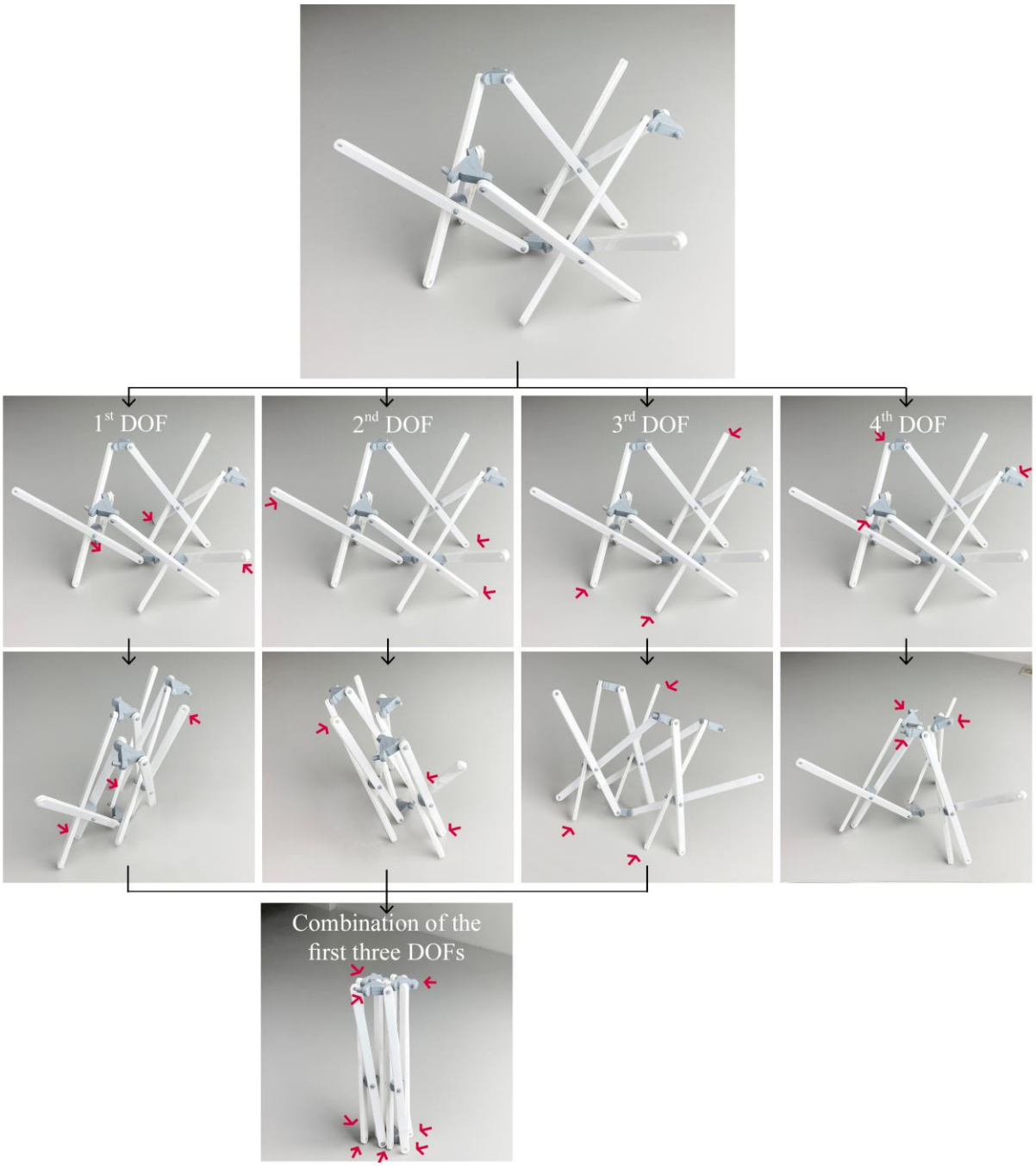


Figure 10. Prototype of a translational assembly using members with unequal segments ($l/k$ = 3/2) and its four types of instantaneous DOFs.

The kinematic behavior of the translational TSU assemblies have potential engineering applications. The multiple DOFs of the translational TSU assemblies lend themselves to reconfigurable mechanisms, such as reconfigurable fixtures and gripper mechanisms.

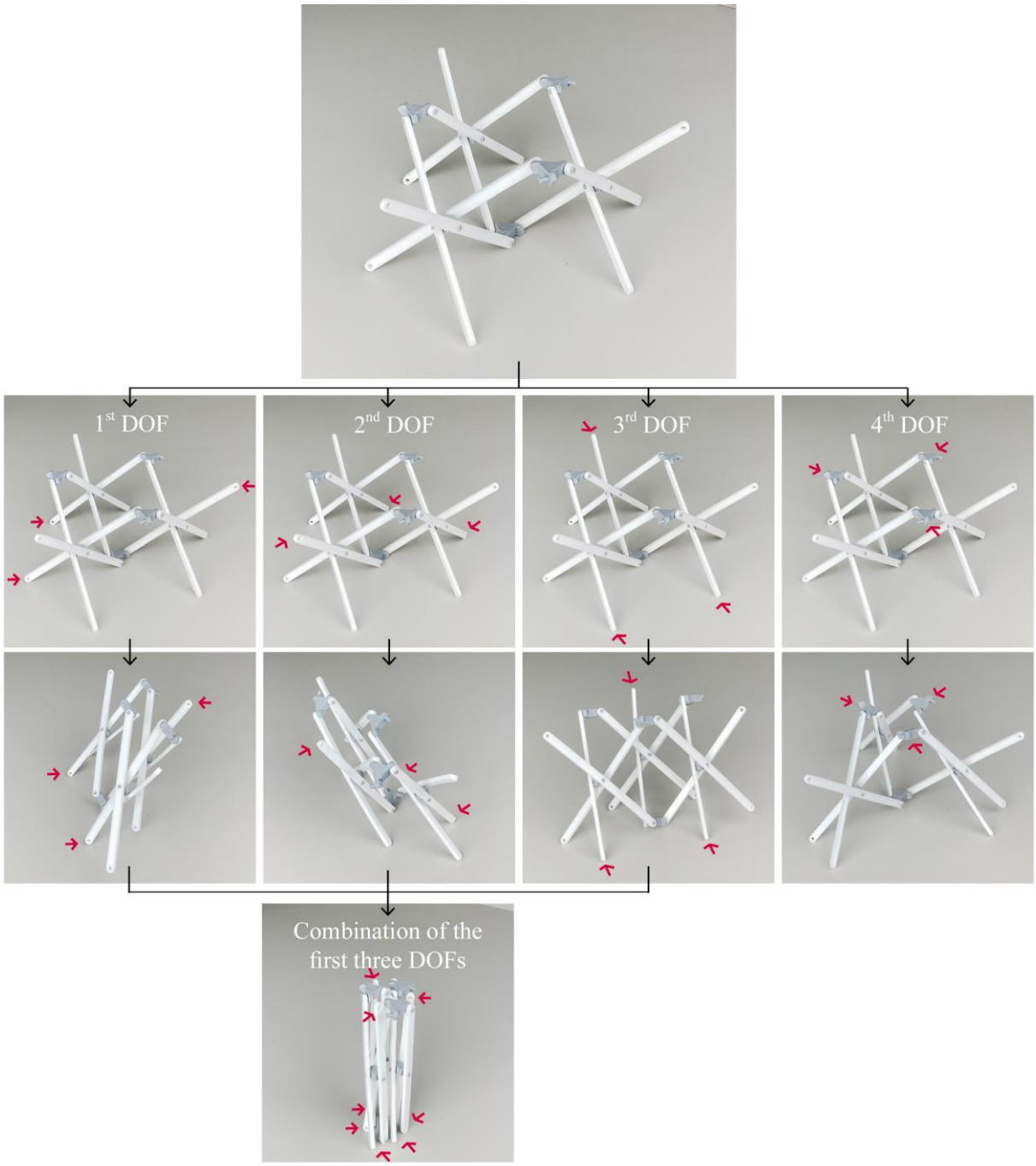


Figure 11. Prototype of a translational assembly using equilateral members and its four types of instantaneous DOFs.

However, for applications where simultaneous movement of the circumferential modules is preferred, such as retractable roof structures, additional links and joints to provide single-DOF movement or special simultaneous actuation means must be considered. A case in point is the *Deployable Traveling Theater* proposed by Piñero using the translational assemblies [30]. He used cables to lock the structure in the three directions for the service configuration. However, according to our analysis, this is not enough because the 4th DOF was not constrained in this

situation. As a result, it can cause large deflections when loads are applied to the frame. In addition, the actuation means should be improved to control such a flexible system.

### *4.2 Prototype of the mirrored assembly*

The physical prototypes of mirrored assembly using members with unequal and equal segments are given in Fig. 12a and b respectively. Both the assemblies can be folded or deployed through a single DOF, which is the same as the results in Section 3. It can be observed from the image that the mirrored assembly approach not only restrains the tripod scissor to be one DOF, but also promotes a curved transformation when using equilateral members, as shown in Fig. 12b. However, when using members with a segment-length ratio of 1.5, the mirrored assembly can unfold horizontally into a flat grid, as shown in Fig. 12a.

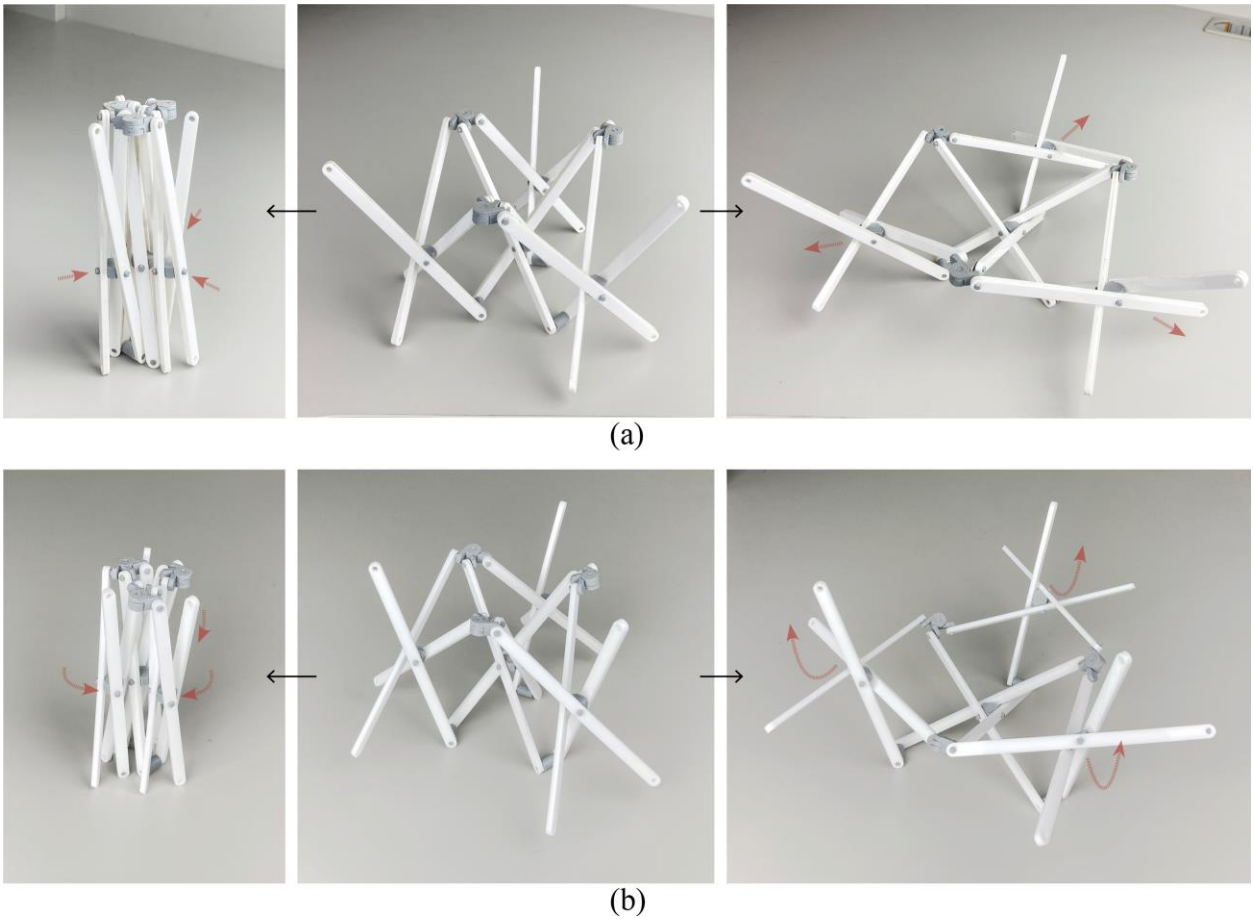


Figure 12. Prototypes of a mirrored assembles with single DOF during their folding and deployment: (a) using members with unequal segments ($l/k$ = 3/2) and (b) using equilateral members.

The single-DOF facilitates control of the mirrored assemblies, making them suitable for kinetic architectures in kinematics, such as emergency shelters and retractable roofs. An example of deployable shelter was presented in [36], where the members are modified so that the assembly can achieve a closed polyhedral form. The single-DOF ease the deployment of the shelter, which can reduce the erection time and require less labor. These merits make it an ideal shelter solution for disaster relief.

## 5. Conclusions

In this paper, the instantaneous mobility of two types of tripod scissor structures was analyzed using screw theory. The study focuses on a configuration in which all the members are deployed at the same angle and all the joint axes are parallel to the same plane. Both the cases with general member geometries (unequal segmental lengths) and special member geometries (equal segmental lengths) were examined. The different kinematic behaviors of the two assembly types have been identified, and the results are

- The translational assemblies using both equal and unequal semi-length members have four instantaneous DOFs, in the given configuration. For the special case (with equal segmental length member), only the 4$^{th}$ DOF is infinitesimal; while for the general case (with unequal segmental length member), at least the 4$^{th}$ DOF is infinitesimal.
- For translational assemblies, different configurations and assembly modes can be obtained from the given configuration. All possible assembly modes of the mechanism could be worked out as a future study.
- The mirrored assemblies using both equal and unequal semi-length members have one DOF.
- And, when using identical member shapes, changing the member's segmental lengths does not influence the mobility of the mirrored assemblies.

This paper primarily examines the mobility of the tripod scissor assemblies. It has the following limitations due to the length of the paper, which should be further investigated in the future. First, this study is limited to the analysis of the instantaneous DOF, while whether these DOFs are finite or not should be examined in the next step. Second, for the translational assemblies with multiple DOFs and motion modes, their instantaneous mobility of different configurations should be further investigated to fully understand the kinematics of this mechanism. Third, for both the translational and mirrored assemblies, only the basic modules are analyzed. Complex problems with an increased number of modules and elements should be studied to verify and improve the formulations and results of the basic assemblies.

## Acknowledgments

The authors appreciate Dr. Liu, Chunxiao for his help with the math problems of this study, and the help of Tarık Kadak, Murat Demirel, Merve Özkahya for the CAD models. This research did not receive any specific grant from funding agencies in the public, commercial, or not-for-profit sectors.

## Appendix A

The screws of the revolute joints, $\$_1$-$\$_{18}$, are given as follows

$$\$_1 = \begin{pmatrix} 0 & -1 & 0 & 0 & 0 & -r_2 \end{pmatrix}^{\mathrm{T}} \tag{A1}$$

$$\$_2 = \begin{pmatrix} \frac{\sqrt{3}}{2} & \frac{1}{2} & 0 & 0 & 0 & -r_2 \end{pmatrix}^{\mathrm{T}} \tag{A2}$$

$$\$_3 = \begin{pmatrix} -\frac{\sqrt{3}}{2} & \frac{1}{2} & 0 & 0 & 0 & -r_2 \end{pmatrix}^{\mathrm{T}} \tag{A3}$$

$$\$_4 = \begin{pmatrix} 0 & -1 & 0 & k\cos\gamma & 0 & -r_2 - k\sin\gamma \end{pmatrix}^{\mathrm{T}} \tag{A4}$$

$$\$_5=\$_{12}=\left(\frac{\sqrt{3}}{2}\quad\frac{1}{2}\quad 0\quad -\frac{k}{2}\cos\gamma\quad\frac{\sqrt{3}}{2}k\cos\gamma\quad\frac{r_2}{2}+\frac{k}{2}\sin\gamma\right)^{\mathrm{T}} \tag{A5}$$

$$\$_6=\$_8=\left(-\frac{\sqrt{3}}{2}\quad\frac{1}{2}\quad 0\quad -\frac{k}{2}\cos\gamma\quad -\frac{\sqrt{3}}{2}k\cos\gamma\quad\frac{r_2}{2}+\frac{k}{2}\sin\gamma\right)^{\mathrm{T}} \tag{A6}$$

$$\$_7=\left(\frac{\sqrt{3}}{2}\quad\frac{1}{2}\quad 0\quad -\frac{k}{2}\cos\gamma\quad\frac{\sqrt{3}}{2}k\cos\gamma\quad -\frac{r_2}{2}-\frac{k}{2}\sin\gamma\right)^{\mathrm{T}} \tag{A7}$$

$$\$_9=\$_{11}=\left(0\quad -1\quad 0\quad k\cos\gamma\quad 0\quad\frac{r_2}{2}+\frac{k}{2}\sin\gamma\right)^{\mathrm{T}} \tag{A8}$$

$$\$_{10}=\left(-\frac{\sqrt{3}}{2}\quad\frac{1}{2}\quad 0\quad -\frac{k}{2}\cos\gamma\quad -\frac{\sqrt{3}}{2}k\cos\gamma\quad -\frac{r_2}{2}-\frac{k}{2}\sin\gamma\right)^{\mathrm{T}} \tag{A9}$$

$$\$_{13}=\$_{16}=\left(\frac{\sqrt{3}}{2}\quad\frac{1}{2}\quad 0\quad -\frac{1}{2}(l+k)\cos\gamma\quad\frac{\sqrt{3}}{2}(l+k)\cos\gamma\quad\frac{r_2}{2}+\left(\frac{k}{2}-l\right)\sin\gamma\right)^{\mathrm{T}} \tag{A10}$$

$$\$_{14}=\$_{17}=\left(0\quad -1\quad 0\quad (l+k)\cos\gamma\quad 0\quad\frac{r_2}{2}+\left(\frac{k}{2}-l\right)\sin\gamma\right)^{\mathrm{T}} \tag{A11}$$

$$\$_{15}=\$_{18}=\left(-\frac{\sqrt{3}}{2}\quad\frac{1}{2}\quad 0\quad -\frac{1}{2}(l+k)\cos\gamma\quad -\frac{\sqrt{3}}{2}(l+k)\cos\gamma\quad\frac{r_2}{2}+\left(\frac{k}{2}-l\right)\sin\gamma\right)^{\mathrm{T}} \tag{A12}$$

## Appendix B

The screws of the revolute joints, $\$'_1$-$\$'_{18}$, are given as follows

$$\$'_1=\left(0\quad -1\quad 0\quad 0\quad 0\quad -r_2\right)^{\mathrm{T}} \tag{B1}$$

$$\$'_2=\left(\frac{\sqrt{3}}{2}\quad\frac{1}{2}\quad 0\quad 0\quad 0\quad -r_2\right)^{\mathrm{T}} \tag{B2}$$

$$\$'_3=\left(-\frac{\sqrt{3}}{2}\quad\frac{1}{2}\quad 0\quad 0\quad 0\quad -r_2\right)^{\mathrm{T}} \tag{B3}$$

$$\$'_4=\left(0\quad -1\quad 0\quad l\cos\gamma\quad 0\quad -r_2-l\sin\gamma\right)^{\mathrm{T}} \tag{B4}$$

$$\$'_5=\$'_{12}=\left(\frac{\sqrt{3}}{2}\quad\frac{1}{2}\quad 0\quad -\frac{1}{2}l\cos\gamma\quad\frac{\sqrt{3}}{2}l\cos\gamma\quad\frac{r_2}{2}+\frac{l}{2}\sin\gamma\right)^{\mathrm{T}} \tag{B5}$$

$$\$'_6=\$'_8=\left(-\frac{\sqrt{3}}{2}\quad\frac{1}{2}\quad 0\quad -\frac{1}{2}l\cos\gamma\quad -\frac{\sqrt{3}}{2}l\cos\gamma\quad\frac{r_2}{2}+\frac{l}{2}\sin\gamma\right)^{\mathrm{T}} \tag{B6}$$

$$\$'_7=\left(\frac{\sqrt{3}}{2}\quad\frac{1}{2}\quad 0\quad -\frac{1}{2}l\cos\gamma\quad\frac{\sqrt{3}}{2}l\cos\gamma\quad -\frac{r_2}{2}-\frac{l}{2}\sin\gamma\right)^{\mathrm{T}} \tag{B7}$$

$$\$'_9=\$'_{11}=\left(0\quad -1\quad 0\quad l\cos\gamma\quad 0\quad\frac{r_2}{2}+\frac{l}{2}\sin\gamma\right)^{\mathrm{T}} \tag{B8}$$

$$\$'_{10}=\left(-\frac{\sqrt{3}}{2}\quad\frac{1}{2}\quad 0\quad -\frac{1}{2}l\cos\gamma\quad -\frac{\sqrt{3}}{2}l\cos\gamma\quad -\frac{r_2}{2}-\frac{l}{2}\sin\gamma\right)^{\mathrm{T}} \tag{B9}$$

$$\$'_{13}=\$'_{16}=\left(\frac{\sqrt{3}}{2}\quad\frac{1}{2}\quad 0\quad -l\cos\gamma\quad \sqrt{3}l\cos\gamma\quad \frac{r_2}{2}-\frac{l}{2}\sin\gamma\right)^{\mathrm{T}} \tag{B10}$$

$$\$'_{14}=\$'_{17}=\left(0\quad -1\quad 0\quad 2l\cos\gamma\quad 0\quad \frac{r_2}{2}-\frac{l}{2}\sin\gamma\right)^{\mathrm{T}} \tag{B11}$$

$$\$'_{15}=\$'_{18}=\left(-\frac{\sqrt{3}}{2}\quad\frac{1}{2}\quad 0\quad -l\cos\gamma\quad -\sqrt{3}l\cos\gamma\quad \frac{r_2}{2}-\frac{l}{2}\sin\gamma\right)^{\mathrm{T}} \tag{B12}$$

## Appendix C

The derivation of Eq. (11) is given as follows: For a mirrored assembly, the addition of the top-end hub causes offsets and hence the upper segment must be shortened to to accommodate it. Here, we use the fully deployed configuration [36] to prove the relationship between the upper segmental length $l$ and its theoretical length $l'$.

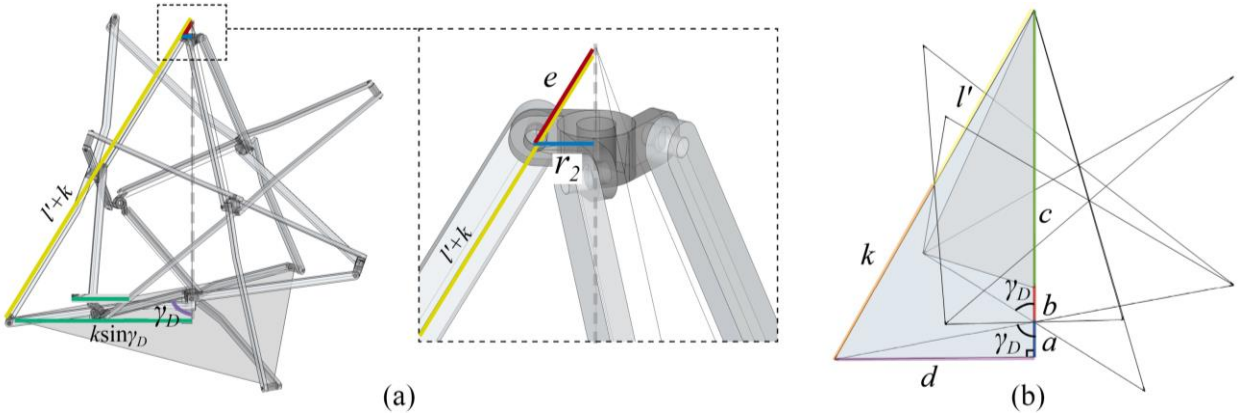


Figure C1. Geometric relationship of a mirrored assembly in the fully deployed configuration.

As shown in Fig. C1a, two similar triangles can be formed in this configuration and their corresponding sides are in equal proportion as

$$\frac{e}{l'+k}=\frac{r_2}{k\sin\gamma_D} \tag{C1}$$

therefore, we have

$$e=\frac{r_2\left(l'+k\right)}{k\sin\gamma_D} \tag{C2}$$

where $\gamma_D$ is determined by $k$ and $l'$. Referring to the right triangle in Fig. C1b, we have

$$(a+b+c)^2+d^2=(k+l')^2 \tag{C3}$$

where

$$a=k\cos\gamma_D \tag{C4.1}$$

$$b=l'\cos\gamma_D \tag{C4.2}$$

$$c=\sqrt{2}l'\sin\gamma_D \tag{C4.3}$$

$$d=k\sin\gamma_D \tag{C4.4}$$

Substituting Eqs. (C4.1)-(C4.4) into Eq. (C3), $\sin\gamma_D$ can be solved. And plug it into Eq. (C2), the value of the shortened distance $e$ can be found. Consequently, the shortened length of the upper

segment is

$$l = l' - e = l' - \frac{r_2(2k - l')}{2\sqrt{2}k}\sqrt{1 + \frac{8(k + l')^2}{(2k - l')^2}} \tag{C5}$$

## Appendix D

The screws of the revolute joints, $\$_m^1$-$\$_m^{30}$, are given as follows

$$\$_m^1 = \begin{pmatrix} q_m^1 & p_m^1 \times q_m^1 \end{pmatrix}^{\mathrm{T}} \tag{D1}$$

$$\$_m^2 = \begin{pmatrix} q_m^2 & p_m^2 \times q_m^2 \end{pmatrix}^{\mathrm{T}} \tag{D2}$$

$$\$_m^3 = \begin{pmatrix} q_m^3 & p_m^3 \times q_m^3 \end{pmatrix}^{\mathrm{T}} \tag{D3}$$

$$\$_m^4 = \begin{pmatrix} \mathbf{R}q_m^1 & (\mathbf{R}p_m^1) \times (\mathbf{R}q_m^1) \end{pmatrix}^{\mathrm{T}} \tag{D4}$$

$$\$_m^5 = \begin{pmatrix} \mathbf{R}q_m^2 & (\mathbf{R}p_m^2) \times (\mathbf{R}q_m^2) \end{pmatrix}^{\mathrm{T}} \tag{D5}$$

$$\$_m^6 = \begin{pmatrix} \mathbf{R}q_m^3 & (\mathbf{R}p_m^3) \times (\mathbf{R}q_m^3) \end{pmatrix}^{\mathrm{T}} \tag{D6}$$

$$\$_m^7 = \begin{pmatrix} \mathbf{RR}q_m^1 & (\mathbf{RR}p_m^1) \times (\mathbf{RR}q_m^1) \end{pmatrix}^{\mathrm{T}} \tag{D7}$$

$$\$_m^8 = \begin{pmatrix} \mathbf{RR}q_m^2 & (\mathbf{RR}p_m^2) \times (\mathbf{RR}q_m^2) \end{pmatrix}^{\mathrm{T}} \tag{D8}$$

$$\$_m^9 = \begin{pmatrix} \mathbf{RR}q_m^3 & (\mathbf{RR}p_m^3) \times (\mathbf{RR}q_m^3) \end{pmatrix}^{\mathrm{T}} \tag{D9}$$

$$\$_m^{10} = \begin{pmatrix} \mathbf{R}_1 q_m^1 & (\mathbf{R}_1 p_m^1 + \mathbf{T}_1) \times (\mathbf{R}_1 q_m^1) \end{pmatrix}^{\mathrm{T}} \tag{D10}$$

$$\$_m^{11} = \begin{pmatrix} \mathbf{R}_1\mathbf{R}q_m^1 & (\mathbf{R}_1\mathbf{R}p_m^1 + \mathbf{T}_1) \times (\mathbf{R}_1\mathbf{R}q_m^1) \end{pmatrix}^{\mathrm{T}} \tag{D11}$$

$$\$_m^{12} = \begin{pmatrix} \mathbf{R}_1\mathbf{R}q_m^3 & (\mathbf{R}_1\mathbf{R}p_m^3 + \mathbf{T}_1) \times (\mathbf{R}_1\mathbf{R}q_m^3) \end{pmatrix}^{\mathrm{T}} \tag{D12}$$

$$\$_m^{13} = \begin{pmatrix} \mathbf{R}_1\mathbf{RR}q_m^1 & (\mathbf{R}_1\mathbf{RR}p_m^1 + \mathbf{T}_1) \times (\mathbf{R}_1\mathbf{RR}q_m^1) \end{pmatrix}^{\mathrm{T}} \tag{D13}$$

$$\$_m^{14} = \begin{pmatrix} \mathbf{R}_1\mathbf{RR}q_m^3 & (\mathbf{R}_1\mathbf{RR}p_m^3 + \mathbf{T}_1) \times (\mathbf{R}_1\mathbf{RR}q_m^3) \end{pmatrix}^{\mathrm{T}} \tag{D14}$$

$$\$_m^{15} = \begin{pmatrix} \mathbf{RR}_1 q_m^1 & (\mathbf{R}(\mathbf{R}_1 p_m^1 + \mathbf{T}_1)) \times (\mathbf{RR}_1 q_m^1) \end{pmatrix}^{\mathrm{T}} \tag{D15}$$

$$\$_m^{16} = \begin{pmatrix} \mathbf{RR}_1\mathbf{R}q_m^1 & (\mathbf{R}(\mathbf{R}_1\mathbf{R}p_m^1 + \mathbf{T}_1)) \times (\mathbf{RR}_1\mathbf{R}q_m^1) \end{pmatrix}^{\mathrm{T}} \tag{D16}$$

$$\$_m^{17} = \begin{pmatrix} \mathbf{RR}_1\mathbf{R}q_m^3 & (\mathbf{R}(\mathbf{R}_1\mathbf{R}p_m^3 + \mathbf{T}_1)) \times (\mathbf{RR}_1\mathbf{R}q_m^3) \end{pmatrix}^{\mathrm{T}} \tag{D17}$$

$$\$_m^{18} = \begin{pmatrix} \mathbf{RR}_1\mathbf{RR}q_m^1 & (\mathbf{R}(\mathbf{R}_1\mathbf{RR}p_m^1 + \mathbf{T}_1)) \times (\mathbf{RR}_1\mathbf{RR}q_m^1) \end{pmatrix}^{\mathrm{T}} \tag{D18}$$

$$\$_m^{19} = \begin{pmatrix} \mathbf{RR}_1\mathbf{RR}q_m^3 & (\mathbf{R}(\mathbf{R}_1\mathbf{RR}p_m^3 + \mathbf{T}_1)) \times (\mathbf{RR}_1\mathbf{RR}q_m^3) \end{pmatrix}^{\mathrm{T}} \tag{D19}$$

$$\$_m^{20} = \begin{pmatrix} \mathbf{RRR}_1 q_m^1 & (\mathbf{RR}(\mathbf{R}_1 p_m^1 + \mathbf{T}_1)) \times (\mathbf{RRR}_1 q_m^1) \end{pmatrix}^{\mathrm{T}} \tag{D20}$$

$$\$_m^{21} = \begin{pmatrix} \mathbf{RRR}_1\mathbf{R}q_m^1 & (\mathbf{RR}(\mathbf{R}_1\mathbf{R}p_m^1 + \mathbf{T}_1)) \times (\mathbf{RRR}_1\mathbf{R}q_m^1) \end{pmatrix}^{\mathrm{T}} \tag{D21}$$

$$\$_m^{22} = \begin{pmatrix} \mathbf{RRR}_1\mathbf{R}q_m^3 & (\mathbf{RR}(\mathbf{R}_1\mathbf{R}p_m^3 + \mathbf{T}_1)) \times (\mathbf{RRR}_1\mathbf{R}q_m^3) \end{pmatrix}^{\mathrm{T}} \tag{D22}$$

$$\$_m^{23} = \begin{pmatrix} \mathbf{RRR}_1\mathbf{RR}q_m^1 & (\mathbf{RR}(\mathbf{R}_1\mathbf{RR}p_m^1 + \mathbf{T}_1)) \times (\mathbf{RRR}_1\mathbf{RR}q_m^1) \end{pmatrix}^{\mathrm{T}} \tag{D23}$$

$$\$_m^{24} = \begin{pmatrix} \mathbf{RRR}_1\mathbf{RR}q_m^3 & (\mathbf{RR}(\mathbf{R}_1\mathbf{RR}p_m^3 + \mathbf{T}_1)) \times (\mathbf{RRR}_1\mathbf{RR}q_m^3) \end{pmatrix}^{\mathrm{T}} \tag{D24}$$

$$\$_m^{25} = \begin{pmatrix} \boldsymbol{q}_m^{25} & \boldsymbol{p}_m^{25} \times \boldsymbol{q}_m^{25} \end{pmatrix}^{\mathrm{T}} \tag{D25}$$

where,

$$\boldsymbol{q}_m^{25} = \begin{pmatrix} 1 & 0 & 2\cot\gamma \end{pmatrix}^{\mathrm{T}} \tag{D25.1}$$

$$\boldsymbol{p}_m^{25} = \begin{pmatrix} -l\sin\gamma - \dfrac{2r_2\cot\gamma}{\sqrt{1+(2\cot\gamma)^2}} & 0 & l\cos\gamma + \dfrac{r_2}{\sqrt{1+(2\cot\gamma)^2}} \end{pmatrix}^{\mathrm{T}} \tag{D25.2}$$

$$\$_m^{26} = \$_m^{25} \tag{D26}$$

$$\$_m^{27} = \begin{pmatrix} \mathbf{R}\boldsymbol{q}_m^{25} & \left(\mathbf{R}\boldsymbol{p}_m^{25}\right) \times \left(\mathbf{R}\boldsymbol{q}_m^{25}\right) \end{pmatrix}^{\mathrm{T}} \tag{D27}$$

$$\$_m^{28} = \$_m^{27} \tag{D28}$$

$$\$_m^{29} = \begin{pmatrix} \mathbf{RR}\boldsymbol{q}_m^{25} & \left(\mathbf{RR}\boldsymbol{p}_m^{25}\right) \times \left(\mathbf{RR}\boldsymbol{q}_m^{25}\right) \end{pmatrix}^{\mathrm{T}} \tag{D29}$$

$$\$_m^{30} = \$_m^{29} \tag{D30}$$

## References


[1] B. Suthar, S. Jung, Design and Bending Analysis of a Metamorphic Parallel Twisted-Scissor Mechanism, J. Mech. Robot. 13 (2021). https://doi.org/10.1115/1.4050813.

[2] Y. Yang, L. Tang, H. Zheng, Y. Zhou, Y. Peng, S. Lyu, Kinematic stability of a 2-DOF deployable translational parallel manipulator, Mech. Mach. Theory. 160 (2021) 104261. https://doi.org/10.1016/j.mechmachtheory.2021.104261.

[3] T. Yang, P. Li, Y. Shen, Y. Liu, Deployable scissor mechanisms derived from non-crossing angulated structural elements, Mech. Mach. Theory. 165 (2021) 104434. https://doi.org/10.1016/j.mechmachtheory.2021.104434.

[4] Y. Liao, Geometric Design of Deployable Antenna Frame Using Hyperboloid Scissor Structure, in: Earth Sp. 2021, American Society of Civil Engineers, Reston, VA, 2021: pp. 1047–1058. https://doi.org/10.1061/9780784483374.097.

[5] N. Zhao, Y. Luo, G. Wang, Y. Shen, A deployable articulated mechanism enabled in-flight morphing aerial gripper, Mech. Mach. Theory. 167 (2022) 104518. https://doi.org/10.1016/j.mechmachtheory.2021.104518.

[6] Y. Akgün, C.J. Gantes, K.E. Kalochairetis, G. Kiper, A novel concept of convertible roofs with high transformability consisting of planar scissor-hinge structures, Eng. Struct. 32 (2010) 2873–2883. https://doi.org/10.1016/j.engstruct.2010.05.006.

[7] S. Krishnan, Y. Liao, Geometric Design of Deployable Spatial Structures Made of Three-Dimensional Angulated Members, J. Archit. Eng. 26 (2020) 04020029. https://doi.org/10.1061/(ASCE)AE.1943-5568.0000416.

[8] X. Shen, Q. Zhang, D.S.-H. Lee, J. Cai, J. Feng, Static Behavior of a Retractable Suspen-Dome Structure, Symmetry (Basel). 13 (2021) 1105. https://doi.org/10.3390/sym13071105.

[9] Y. Zhou, Q. Zhang, W. Jia, D.S. Lee, J. Cai, J. Feng, Mechanical behavior of elastic telescopic rods for morphing scissor structures, J. Build. Eng. 56 (2022) 104734. https://doi.org/10.1016/j.jobe.2022.104734.

[10] J.J. Moy, C.S. Tan, S. Mohammad, A.R.Z. Abidin, State-of-Art review on deployable scissor structure in construction, Structures. 42 (2022) 160–180. https://doi.org/10.1016/j.istruc.2022.05.084.

[11] T. Langbecker, Kinematic Analysis of Deployable Scissor Structure s, Int. J. Sp. Struct. 14 (1999) 1–15. https://doi.org/10.1260/0266351991494650.

[12] F. Escrig, J.P. Valcárel, J. Sánchez, Roofing Geometry of Deployable X-Frames, Int. J. Sp. Struct. 13 (1998) 1–12. https://doi.org/10.1177/026635119801300101.

[13] C. Hoberman, Reversibly expandable doubly-curved truss structure, U.S. Patent 4,942,700, 1990.

[14] J. Patel, G.K. Ananthasuresh, A kinematic theory for radially foldable planar linkages, Int. J. Solids Struct. 44 (2007) 6279–6298. https://doi.org/10.1016/j.ijsolstr.2007.02.023.

[15] Y. Chen, L. Fan, J. Feng, Kinematic of symmetric deployable scissor-hinge structures with integral mechanism mode, Comput. Struct. 191 (2017) 140–152. https://doi.org/10.1016/j.compstruc.2017.06.006.

[16] J.S. Dai, D. Li, Q. Zhang, G. Jin, Mobility analysis of a complex structured ball based on mechanism decomposition and equivalent screw system analysis, Mech. Mach. Theory. 39 (2004) 445–458. https://doi.org/10.1016/j.mechmachtheory.2003.12.004.

[17] D. Mao, Y. Luo, Z. You, Planar closed loop double chain linkages, Mech. Mach. Theory. 44 (2009) 850–859. https://doi.org/10.1016/j.mechmachtheory.2008.04.005.

[18] J.-S. Zhao, F. Chu, Z.-J. Fing, The mechanism theory and application of deployable structures based on SLE, Mech. Mach. Theory. 44 (2009) 324–335. https://doi.org/https://doi.org/10.1016/j.mechmachtheory.2008.03.014.

[19] J. Cai, Y. Xu, J. Feng, Kinematic analysis of Hoberman's Linkages with the screw theory, Mech. Mach. Theory. 63 (2013) 28–34. https://doi.org/10.1016/j.mechmachtheory.2013.01.004.

[20] J. Cai, X. Deng, J. Feng, Y. Xu, Mobility analysis of generalized angulated scissor-like elements with the reciprocal screw theory, Mech. Mach. Theory. 82 (2014) 256–265. https://doi.org/10.1016/j.mechmachtheory.2014.07.011.

[21] Y. Sun, S. Wang, J. Li, C. Zhi, Mobility analysis of the deployable structure of SLE based on screw theory, Chinese J. Mech. Eng. 26 (2013) 793–800. https://doi.org/10.3901/CJME.2013.04.793.

[22] Y. Sun, S. Wang, J.K. Mills, C. Zhi, Kinematics and dynamics of deployable structures with scissor-like-elements based on screw theory, Chinese J. Mech. Eng. 27 (2014) 655–662. https://doi.org/10.3901/CJME.2014.0519.098.

[23] B. Han, Y. Xu, J. Yao, D. Zheng, Y. Li, Y. Zhao, Design and analysis of a scissors double-ring truss deployable mechanism for space antennas, Aerosp. Sci. Technol. 93 (2019) 105357. https://doi.org/10.1016/j.ast.2019.105357.

[24] B. Han, D. Zheng, Y. Xu, J. Yao, Y. Zhao, Kinematic Characteristics and Dynamics Analysis of an Overconstrained Scissors Double-Hoop Truss Deployable Antenna Mechanism Based on Screw Theory, IEEE Access. 7 (2019) 140755–140768.

https://doi.org/10.1109/ACCESS.2019.2930101.

[25] Y. Wang, Q. Zhang, X. Zhang, J. Cai, C. Jiang, Y. Xu, J. Feng, Analytical and numerical analysis of mobility and kinematic bifurcation of planar linkages, Int. J. Non. Linear. Mech. 145 (2022) 104110. https://doi.org/10.1016/j.ijnonlinmec.2022.104110.

[26] R. Liu, R. Li, Y.-A. Yao, Reconfigurable deployable Bricard-like mechanism with angulated elements, Mech. Mach. Theory. 152 (2020) 103917. https://doi.org/10.1016/j.mechmachtheory.2020.103917.

[27] R. Liu, R. Li, Y. Yao, X. Ding, A reconfigurable deployable spatial 8R-like mechanism consisting of four angulated elements connected by R joints, Mech. Mach. Theory. 179 (2023) 105103. https://doi.org/10.1016/j.mechmachtheory.2022.105103.

[28] Q. Meng, X.-J. Liu, F. Xie, Structure design and kinematic analysis of a class of ring truss deployable mechanisms for satellite antennas based on novel basic units, Mech. Mach. Theory. 174 (2022) 104881. https://doi.org/10.1016/j.mechmachtheory.2022.104881.

[29] Q. Meng, F. Xie, R. Tang, X.-J. Liu, Deployable polyhedral mechanisms with radially reciprocating motion based on novel basic units and an additive-then-subtractive design strategy, Mech. Mach. Theory. 181 (2023) 105174. https://doi.org/10.1016/j.mechmachtheory.2022.105174.

[30] P.E. Piñero, Three dimensional reticular structure, US Patent 3,185,164, 1965.

[31] F. Escrig, Expandable Space Structures, Int. J. Sp. Struct. 1 (1985) 79–91. https://doi.org/10.1177/026635118500100203.

[32] Y. Akgün, C.J. Gantes, W. Sobek, K. Korkmaz, K. Kalochairetis, A novel adaptive spatial scissor-hinge structural mechanism for convertible roofs, Eng. Struct. 33 (2011) 1365–1376. https://doi.org/10.1016/j.engstruct.2011.01.014.

[33] C. Ramos-Jaime, J. Sánchez-Sánchez, Hyperboloid Modules for Deployable Structures, Nexus Netw. J. 22 (2020) 309–328. https://doi.org/10.1007/s00004-019-00459-y.

[34] J. Pérez-Valcárcel, F. Suárez-Riestra, M. Muñoz-Vidal, I. López-César, M.J. Freire-Tellado, A new reciprocal linkage for expandable emergency structures, Structures. 28 (2020) 2023–2033. https://doi.org/10.1016/j.istruc.2020.10.008.

[35] J. Pérez-Valcárcel, M. Muñoz-Vidal, F. Suárez-Riestra, I.R. López-César, M.J. Freire-Tellado, Deployable cylindrical vaults with reciprocal linkages for emergency buildings, Structures. 33 (2021) 4461–4474. https://doi.org/10.1016/j.istruc.2021.06.094.

[36] Y. Liao, S. Krishnan, Geometric design and kinematics of spatial deployable structures using tripod-scissor units, Structures. 38 (2022) 323–339. https://doi.org/10.1016/j.istruc.2022.01.009.

[37] Y. Liao, Modeling and analysis of tripod-scissor deployable structures using mirrored assembly methods, in: S. Behnejad, G. Parke, O. Samavari (Eds.), Proc. IASS Annu. Symp. IASS 2020/21 Surrey Symp. Deployable, Foldable Tensegrity Struct., Surrey, 2021: pp. 1–12.

[38] A. Pérez-Egea, P. García Martínez, M. Peña Fernández-Serrano, P.M. Jiménez Vicario, M.A. Ródenas-López, The influence of joint eccentricity on the foldability of four

deployable structure systems, Int. J. Sp. Struct. 37 (2022) 3–21. https://doi.org/10.1177/09560599211048441.

[39] B. Suthar, S. Jung, Design of a Novel Twisted-Scissor Structure for a Foldable Robot Arm, in: 2021 18th Int. Conf. Ubiquitous Robot., IEEE, 2021: pp. 139–143. https://doi.org/10.1109/UR52253.2021.9494707.

[40] S. Yang, J.S. Dai, Y. Jin, R. Fu, Finite displacement screw-based group analysis of 3PRS parallel mechanisms, Mech. Mach. Theory. 171 (2022) 104727. https://doi.org/10.1016/j.mechmachtheory.2022.104727.

[41] J.S. Dai, Z. Huang, H. Lipkin, Mobility of Overconstrained Parallel Mechanisms, J. Mech. Des. 128 (2006) 220–229. https://doi.org/10.1115/1.1901708.

[42] Z. Huang, J. Liu, D. Zeng, A general methodology for mobility analysis of mechanisms based on constraint screw theory, Sci. China Ser. E Technol. Sci. 52 (2009) 1337–1347. https://doi.org/10.1007/s11431-008-0219-1.

[43] S. Boztaş, G. Kiper, Enumeration and instantaneous mobility analysis of a class of 3-UPU parallel manipulators with equilateral triangular platforms, Robotica. 40 (2022) 1538–1569. https://doi.org/10.1017/S0263574721001259.

[44] X. Kang, H. Feng, J.S. Dai, H. Yu, High-order based revelation of bifurcation of novel Schatz-inspired metamorphic mechanisms using screw theory, Mech. Mach. Theory. 152 (2020) 103931. https://doi.org/10.1016/j.mechmachtheory.2020.103931.

[45] H. Lei, X. Kang, B. Li, Reconfiguration characteristic revelation of multiple metamorphic mechanisms based on geometric morphology of screw systems, Mech. Mach. Theory. 184 (2023) 105285. https://doi.org/10.1016/j.mechmachtheory.2023.105285.

[46] A. Müller, A Screw Approach to the Approximation of the Local Geometry of the Configuration Space and of the Set of Configurations of Certain Rank of Lower Pair Linkages, J. Mech. Robot. 11 (2019) 1–9. https://doi.org/10.1115/1.4042545.

[47] A. Müller, Screw and Lie group theory in multibody kinematics, Multibody Syst. Dyn. 43 (2018) 37–70. https://doi.org/10.1007/s11044-017-9582-7.

[48] J. Pérez-Valcárcel, M. Muñoz-Vidal, F. Suárez-Riestra, I.R. López-César, M.J. Freire-Tellado, Deployable bundle modulus structures with reciprocal linkages for emergency buildings, Eng. Struct. 244 (2021) 112803. https://doi.org/10.1016/j.engstruct.2021.112803.

[49] F. Escrig, J.P. Valcarcel, Geometry of Expandable Space Structures, Int. J. Sp. Struct. 8 (1993) 71–84. https://doi.org/10.1177/026635119300800l-208.

[50] J. Pérez-Valcárcel, I.R. López-César, M. Muñoz-Vidal, M.J. Freire-Tellado, F. Suárez-Riestra, Deployable tubular bar structures with laterally confined flattened ends, Structures. 55 (2023) 112–122. https://doi.org/10.1016/j.istruc.2023.06.045.

[51] A. Müller, Kinematic topology and constraints of multi-loop linkages, Robotica. 36 (2018) 1641–1663. https://doi.org/10.1017/S0263574718000619.

[52] G. Wei, X. Ding, J.S. Dai, Mobility and Geometric Analysis of the Hoberman Switch-Pitch Ball and Its Variant, J. Mech. Robot. 2 (2010) 031010.

https://doi.org/10.1115/1.4001730.

[53] K. Wohlhart, Degrees of shakiness, Mech. Mach. Theory. 34 (1999) 1103–1126. https://doi.org/10.1016/S0094-114X(98)00027-5.

[54] A. Müller, Local Kinematic Analysis of Closed-Loop Linkages—Mobility, Singularities, and Shakiness, J. Mech. Robot. 8 (2016) 1–11. https://doi.org/10.1115/1.4032778.

[55] F. Maden, Y. Akgün, G. Kiper, Ş. Gür, M. Yar, K. Korkmaz, A Critical Review on Classification and Terminology of Scissor Structures, J. Int. Assoc. Shell Spat. Struct. 60 (2019) 47–64. https://doi.org/10.20898/j.iass.2019.199.029.